



**HAL**  
open science

# Lax–Wendroff Schemes with Polynomial Extrapolation and Simplified Lax–Wendroff Schemes for Dispersive Waves: A Comparative Study

Aurore Cauquis, Mario Ricchiuto, Philippe Heinrich

► **To cite this version:**

Aurore Cauquis, Mario Ricchiuto, Philippe Heinrich. Lax–Wendroff Schemes with Polynomial Extrapolation and Simplified Lax–Wendroff Schemes for Dispersive Waves: A Comparative Study. *Water Waves*, 2022, 10.1007/s42286-022-00060-w . hal-03723732

**HAL Id: hal-03723732**

**<https://inria.hal.science/hal-03723732>**

Submitted on 2 Aug 2022

**HAL** is a multi-disciplinary open access archive for the deposit and dissemination of scientific research documents, whether they are published or not. The documents may come from teaching and research institutions in France or abroad, or from public or private research centers.

L'archive ouverte pluridisciplinaire **HAL**, est destinée au dépôt et à la diffusion de documents scientifiques de niveau recherche, publiés ou non, émanant des établissements d'enseignement et de recherche français ou étrangers, des laboratoires publics ou privés.

# Lax-Wendroff schemes with polynomial extrapolation and simplified Lax-Wendroff schemes for dispersive waves: a comparative study

Aurore Cauquis<sup>\*"</sup>, Mario Ricchiuto<sup>"</sup>, Philippe Heinrich<sup>\*</sup>

<sup>\*</sup>CEA, DAM, DIF, F-91297, Arpajon, France

<sup>"</sup>INRIA, Univ. Bordeaux, CNRS, Bordeaux INP, IMB, UMR 5251,

200 Avenue de la Vieille Tour, 33405 Talence cedex, France

October 12, 2021

## Abstract

One of the features of Boussinesq type models for dispersive wave propagation is the presence of mixed spatial/temporal derivatives in the partial differential system. This is a critical point in the design of the time marching strategy, as the cost of inverting the algebraic equations arising from the discretization of these mixed terms may result in a non-negligible overhead. In this paper, we propose novel approaches based on the classical Lax-Wendroff (LW) strategy to achieve single step high order schemes in time. To reduce the cost of evaluating the complex correction terms arising in the Lax-Wendroff procedure for Boussinesq equations, we propose several simplified strategies which allow to reduce the computational time at fixed accuracy. To evaluate these qualities, we perform a spectral analysis to assess the dispersion and damping error. We then evaluate the schemes on several benchmarks involving dispersive propagation over flat and non-flat bathymetries, and perform numerical grid convergence studies on two of them. Our results show a potential for a CPU reduction between 35% and 40% to obtain accuracy levels comparable to those of the classical RK3 method.

## 1 Introduction

In France, tsunami warning is currently based on the operational code used by the Tsunami Warning Centers in French Polynesia and mainland France, which solves shallow water equations. In this context, computational time is a critical factor. As shown in previous studies [1] [2] [3], the propagation of transoceanic tsunamis is dispersive and shallow water models, which are generally used in tsunami warning context, may produce inaccurate results.

Most recent numerical models of tsunami propagation take frequency dispersion into account. These ones are based either on Boussinesq-type equations [4] [5] or on nonlinear shallow water equations coupled with a pressure Poisson equation [6] [7].

In the first category, standard Boussinesq equations [8] assume that both nonlinearity and frequency dispersion are weak. The validity domain of Boussinesq equations has been extended to deeper water depths and two new formulations introduced by Madsen and Srensen [9] and Nwogu

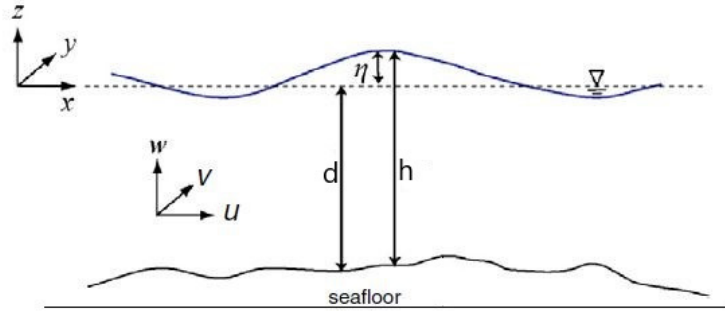


Figure 1: Definition of variables

[10] are widely in use. Finally, a "fully-nonlinear" formulation eliminating the weak nonlinearity assumption has been introduced ([11], [4], [12]) which extends the applicability of Boussinesq equations to strongly nonlinear waves and to the surf zone.

Numerical approaches include a wide range of Finite Difference (FD) or Finite Volume (FV) formulations. In order to deal with strongly nonlinear waves, most recent numerical models use a hybrid method which combines FV and FD schemes ([13], [14], [4], [15], [16]). The FV formulation with shock-capturing capabilities is used for the discretization of the continuity equation and part of the momentum equations (acceleration term and convective momentum terms). The dispersive terms are discretized by a FD formulation. Since dispersive terms in Boussinesq equations contain third-order spatial derivatives, a high-order numerical scheme (with a 4th-order accuracy) is generally developed in order to minimize the truncation error. As regards temporal schemes, third-order Adams-Basforth methods or third-order Runge-Kutta methods are generally adopted.

These latter models are computationally expensive and their application to real-world tsunami propagations might not be always justifiable. We propose in this study to solve the weakly nonlinear Boussinesq equations with extended dispersion and written in a non-conservative form [17]. A new formulation of these equations is written and results in solving an additional equation where no time discretization is required. This formulation allows for a thorough analysis of truncature errors and of their effects on both the accuracy of results and the computational time. The aim of this paper is to study the balance between computational speed and numerical errors introduced by Boussinesq models through a set of test cases.

To this end, we propose novel time stepping approaches based on the classical Lax-Wendroff strategy to achieve single step high order schemes in time. To reduce the cost of evaluating the complex correction terms arising in the LW procedure for Boussinesq equations, we propose several simplified strategies which allow to reduced the computational time at fixed accuracy. This is verified quantitatively both using a linear spectral analysis of the dispersion error, and benchmarks involving dispersive propagation on flat and non-flat bathymetries.

The paper is organized as follows. In Section 2, we present the model equations. The time marching schemes, and in particular the Lax Wendroff methods we propose, are described in Section 3. In Section 4, a spectral analysis is performed to compare the dispersion and damping of the different approaches considered. In Section 5, the schemes are compared for four benchmarks: the propagation of a linear gaussian wave, of a solitary wave, of an undular bore and of a dambreak-generated wave.

## 2 Weakly-nonlinear and weakly dispersive wave propagation model

This section is devoted to the presentation of the 1D Boussinesq equations used in this work and their dimensionless formulation.

We start from the Boussinesq equations written in a non-conservative form [17] :

$$\begin{cases} \partial_t \eta + \partial_x(hu) & = 0 \\ \partial_t \left( u - \frac{du}{2} \partial_{xx} d - d \partial_x d \partial_x u - \alpha d^2 \partial_{xx} u \right) + g \partial_x (\eta - \beta d^2 \partial_{xx} \eta) + u \partial_x u & = 0 \end{cases}$$

where  $\eta$  is the surface elevation above the still water level,  $d$  is the bathymetry,  $h = \eta + d$  is the water depth,  $u$  is the velocity in the x-direction and  $g = 9.81 \text{ m s}^{-2}$  (Fig 1).  $\alpha$  and  $\beta$  are constants associated to the dispersion [18].

We then use Nwogu's nondimensional parameters [10], denoting the dimensional variables with a prime:

- $u' = \epsilon c_0 w$  where  $\epsilon = a_0/d_0$  is the nonlinearity parameter
- $x' = xl$
- $t' = tl/c_0$
- $\eta' = a_0 \zeta$
- $d' = d_0 d$
- $h' = \eta' + d' = d_0(\epsilon \zeta + d) = d_0 H$

where  $c_0 = \sqrt{gd_0}$ ,  $d_0$  is a given depth,  $l$  is a characteristic length and  $a_0$  a characteristic amplitude.

We obtain the dimensionless system involving the frequential dispersion parameter  $\mu = d_0/l$  :

$$\begin{cases} \partial_t \zeta + \epsilon \partial_x(\zeta w) + \partial_x(dw) & = 0 \\ \partial_t \left( w - \frac{d\mu^2}{2} w \partial_{xx} d - \mu^2 d \partial_x d \partial_x w - \alpha \mu^2 d^2 \partial_{xx} w \right) + \epsilon w \partial_x w + \partial_x(\zeta - \beta \mu^2 d^2 \partial_{xx} \zeta) & = 0 \end{cases}$$

This system can be reformulated by introducing  $\xi$  and  $\phi$  :

$$\begin{cases} \partial_t \zeta + \partial_x(Hw) & = 0 \\ \partial_t \xi + \partial_x \phi & = -\partial_x \left( \mu^2 d \partial_x d \partial_x \zeta + \mu^2 \frac{d}{2} \partial_{xx} d \zeta + \frac{\epsilon w^2}{2} \right) \\ \xi & = w - \alpha \mu^2 d^2 \partial_{xx} w - \mu^2 d \partial_x d \partial_x w - \frac{\mu^2 d}{2} \partial_{xx} dw \\ \phi & = \zeta - \beta \mu^2 d^2 \partial_{xx} \zeta - \mu^2 d \partial_x d \partial_x \zeta - \frac{\mu^2 d}{2} \partial_{xx} d \zeta \end{cases}$$

The Boussinesq equations can be finally recast in the following form featuring a system with a forcing term obtained from an auxiliary elliptic problem: :

$$\begin{cases} \partial_t \zeta + \partial_x(Hw) & = 0 \\ \partial_t w + \partial_x \zeta & = \varphi \\ \varphi & = \mu^2 \beta \partial_x(d^2 \partial_{xx} \zeta) + \mu^2 d \left( \alpha d \partial_{xxt} w + \partial_x d \partial_{xt} w + \frac{1}{2} \partial_{xx} d \partial_t w \right) - \partial_x \left( \frac{\epsilon w^2}{2} \right) \end{cases}$$

Note that the nonlinear term  $\epsilon w^2/2$  in the above equation can also be kept in the left hand side of the second equations rather than in the definition of  $\varphi$  so that neglecting  $\varphi$  would reduce the model to the shallow water equations. This choice is relevant when the limit system ( $\mu^2 = 0$ ) is considered. In this work, this choice is not relevant as we do not consider this limit. In practice we keep the linear form of the left hand side of the momentum equation.

Finally, combining the second and third equations we end with :

$$\partial_t \zeta + \partial_x(Hw) = 0 \quad (1)$$

$$\partial_t w + \partial_x \zeta = \varphi \quad (2)$$

$$\left(1 - \frac{\mu^2 d}{2} \partial_{xx} d\right) \varphi - \mu^2 d \partial_x d \partial_x \varphi - \mu^2 \alpha d^2 \partial_{xx} \varphi = -\mu^2 R(d, \zeta) - \epsilon w \partial_x w \quad (3)$$

where  $R(d, \zeta) = d \left( \frac{1}{2} \partial_{xx} d \partial_x \zeta + (1 - 2\beta) \partial_x d \partial_{xx} \zeta + \gamma d \partial_{xxx} \zeta \right)$ . Remember that  $\zeta$  is the dimensionless surface elevation,  $w$  is the dimensionless velocity in the x-direction,  $d$  is the dimensionless water depth and  $\gamma = \alpha - \beta$ . In the following, we speak of standard Boussinesq system when  $\alpha=1/3$  and  $\beta=0$  [8]. When  $\alpha=0.39$  and  $\beta = 0.057$ , the system corresponds to the frequency enhanced Boussinesq equations of [11].

### 3 Time integration strategies

In this paper, we aim at solving the Boussinesq equations with an efficient centered spatial discretization coupled with a time stepping based on a Lax-Wendroff approach. To obtain computationally efficient, yet accurate, schemes we use two main ideas. The first is to couple the spatial error and the truncation error of the Taylor series expansion in time, using the Lax-Wendroff strategy. The second is to couple this expansion with appropriately chosen polynomial extrapolation in time, allowing for an efficient high order discretization in time. As a reference, we use first, second, and third order explicit Runge-Kutta methods. Note that Filippini et al. 2015 [19] has shown that this method has a lower dispersion error compared to the classical fourth order Adams-Bashfort/Adams-Moulton predictor corrector [11].

#### 3.1 Runge-Kutta schemes

For these schemes, mass and momentum equations (Eq 1 and 2) are written in the form  $\partial_t U = L(U)$  where  $U = (\zeta, w)^T$  and  $L(U) = (-\partial_x(Hw), \varphi - \partial_x \zeta)^T$ .

The explicit Euler scheme consists in replacing  $\partial_t U$  by  $(U^{n+1} - U^n)/\Delta t$ ,  $\Delta t$  being the time step. Note that every evaluation of  $L$  requires the calculation of  $\varphi$  from Eq 3, which requires the inversion of the matrix arising from the discretization of the elliptic problem.

The explicit Euler scheme is written as :

$$U^{n+1} = U^n + \Delta t L(U^n)$$

The RK2 and RK3 schemes are defined as:

$$\left\{ \begin{array}{l} U^{n+\frac{1}{2}} = U^n + \frac{\Delta t}{2} L(U^n) \\ U^{n+1} = U^n + \Delta t L(U^{n+\frac{1}{2}}) \end{array} \right. \text{ and } \left\{ \begin{array}{l} U^p = U^n + \Delta t L(U^n) \\ U^{2p} = \frac{3}{4} U^n + \frac{1}{4} U^p + \frac{\Delta t}{4} L(U^p) \\ U^{n+1} = \frac{1}{3} U^n + \frac{2}{3} U^{2p} + \frac{2\Delta t}{3} L(U^{2p}) \end{array} \right.$$

In the second and third-order Runge-Kutta schemes, the calculation of  $\varphi$  (Eq 3) requires two and three matrix inversions, respectively.

### 3.2 Lax-Wendroff schemes

We perform a truncated Taylor series development to approximate the unknowns at time  $t^{n+1} = (n + 1) \times \Delta t$ , and approximate the temporal derivatives with the aid of the underlying Partial Differential Equations by replacing them with spatial derivatives using Eq 1 and 2. The resulting differential expressions are then discretized by efficient central differences. Let us start from the truncated Taylor series (the third order case is considered, which is the most general case studied here):

$$\zeta^{n+1} = \zeta^n + \Delta t \partial_t \zeta^n + \Delta t^2 / 2 \times \partial_{tt} \zeta^n + \Delta t^3 / 6 \times \partial_{ttt} \zeta^n \quad (4)$$

$$w^{n+1} = w^n + \Delta t \partial_t w^n + \Delta t^2 / 2 \times \partial_{tt} w^n + \Delta t^3 / 6 \times \partial_{ttt} w^n \quad (5)$$

Simple calculations show that the time derivatives required in the above update have the following form:

$$\partial_t \zeta^n = -\partial_x \{Hw\}^n \quad (6)$$

$$\partial_{tt} \zeta^n = \partial_x \{\epsilon w \partial_x (Hw) + H(\partial_x \zeta - \varphi)\}^n \quad (7)$$

$$\partial_{ttt} \zeta^n = \partial_x \{2\epsilon \partial_x (Hw)(-\partial_x \zeta + \varphi) + \epsilon w \partial_x [H(-\partial_x \zeta + \varphi + w)] - h(\partial_{xx}(Hw) + \psi)\}^n \quad (8)$$

$$\partial_t w^n = -(\partial_x \zeta - \varphi)^n \quad (9)$$

$$\partial_{tt} w^n = (\partial_x (Hw) + \psi)^n \quad (10)$$

$$\partial_{ttt} w^n = -\{\partial_x [\epsilon w \partial_x (Hw) + H(\partial_x \zeta - \varphi)] - \theta\}^n \quad (11)$$

In the expressions above, we have introduced the auxiliary variables  $\psi := \partial_t \varphi$  and  $\theta := \partial_{tt} \varphi$ . Combining the truncated series and these expressions, we see that a fully second order approximation (second order in  $\zeta$  and  $w$ ) already requires the computation of both  $\varphi^n$  and  $\psi^n$ , and that an approximation of  $\varphi^n$ ,  $\psi^n$ , and  $\theta^n$  is necessary for third order accuracy in time.

For constant bathymetries,  $\psi$  and  $\theta$  are calculated by taking the time derivatives of Eq 3, which provides the auxiliary elliptic systems:

$$\left(1 - \frac{\mu^2 d}{2} \partial_{xx} d\right) \varphi - \mu^2 d \partial_x d \partial_x \varphi - \mu^2 \alpha d^2 \partial_{xx} \varphi = -\mu^2 R(d, \zeta) - \epsilon w \partial_x w \quad (12)$$

$$\left(1 - \frac{\mu^2 d}{2} \partial_{xx} d\right) \psi - \mu^2 d \partial_x d \partial_x \psi - \mu^2 \alpha d^2 \partial_{xx} \psi = -\mu^2 R(d, \partial_t \zeta) - \epsilon \partial_t (w \partial_x w) \quad (12)$$

$$\left(1 - \frac{\mu^2 d}{2} \partial_{xx} d\right) \theta - \mu^2 d \partial_x d \partial_x \theta - \mu^2 \alpha d^2 \partial_{xx} \theta = -\mu^2 R(d, \partial_{tt} \zeta) - \epsilon \partial_{tt} (w \partial_x w) \quad (13)$$

where the temporal derivatives of  $\zeta$  and  $w$  are replaced by time-independent expressions. Complete expressions are detailed in Annex A for an arbitrary bottom.

The resolution of these new equations results in calculating 4th and 5th spatial derivatives and in inverting more matrices. This gives a numerical scheme which theoretically has the same accuracy of the third and second order RK methods, and comparable computational cost concerning the number of linear systems inverted.

Our objective is to propose strategies to side-step these computations defining more efficient approaches. In order to reduce the computational time, an alternative solution is to calculate approximated time derivatives of  $\varphi$ . Eight different approximations (associated to eight numerical schemes) are proposed in this paper.

### 3.3 Polynomial extrapolation and finite differences in time

We make the observation that the order in time sought can be preserved by replacing the various time derivatives by approximations of an appropriate order. In particular, we can consider the modified update that reads:

$$\begin{cases} \zeta^{n+1} &= \zeta^n + \Delta t \partial_t \zeta^n + \frac{\Delta t^2}{2} \partial_{tt} \zeta^n + \frac{\Delta t^3}{6} \partial_{ttt} \zeta^n \\ w^{n+1} &= w^n + \Delta t \partial_t w^n + \frac{\Delta t^2}{2} \partial_{tt} w^n + \frac{\Delta t^3}{6} \partial_{ttt} w^n \end{cases}$$

where second and third order of accuracy are guaranteed under the following approximation constraints:

$$\begin{cases} \partial_t(\cdot) &= \tilde{\partial}_t(\cdot) + \mathcal{O}(\Delta t^2) \\ \partial_{tt}(\cdot) &= \tilde{\partial}_{tt}(\cdot) + \mathcal{O}(\Delta t) \end{cases}$$

for second order in time and

$$\begin{cases} \partial_t(\cdot) &= \tilde{\partial}_t(\cdot) + \mathcal{O}(\Delta t^3) \\ \partial_{tt}(\cdot) &= \tilde{\partial}_{tt}(\cdot) + \mathcal{O}(\Delta t^2) \\ \partial_{ttt}(\cdot) &= \tilde{\partial}_{ttt}(\cdot) + \mathcal{O}(\Delta t) \end{cases}$$

for third order in time. We have denoted by  $\tilde{\partial}$  a discrete approximation of the temporal derivative  $\partial$  with a certain truncation. The above systems summarize the accuracy constraints necessary for each derivative order for the truncated Taylor series development to meet the required second and third order of accuracy.

This suggests two approaches to obtain approximations of the  $\psi$  and  $\theta$  terms in order to avoid the additional linear system inversions.

The first is based on backward polynomial interpolation, and differentiation, which provides the following first and second order approximations:

$$\psi_{e_1}^n = \frac{\varphi^n - \varphi^{n-1}}{\Delta t}, \psi_{e_2}^n = \frac{3\varphi^n - 4\varphi^{n-1} + \varphi^{n-2}}{2\Delta t} \text{ and } \theta_e^n = \frac{\varphi^n - 2\varphi^{n-1} + \varphi^{n-2}}{\Delta t^2},$$

where we recall that a first order approximation of  $\theta$  is sufficient to guarantee the formal third order of accuracy in time. We refer to this approach as the extrapolated method, and use the subscript  $e$  to denote the associated schemes.

The second is based on an iterative segregated solution strategy. We refer to this approach as the segregated/implicit method, and use the subscript  $si$  to denote the associated schemes. At second order, we first compute  $\zeta^{n+1}$ , which only requires the knowledge of  $\varphi^n$  (Eqs 4, 6, 7 and 8). We then evaluate  $\varphi^{n+1}$  using Eq 3, and set

$$\psi_{si_2}^n = \frac{\varphi^{n+1} - \varphi^{n-1}}{2\Delta t}.$$

Two equivalent first order approximations are obtained by setting

$$\psi_{si_1}^n = \frac{\varphi^{n+1} - \varphi^n}{\Delta t} \text{ or } \psi_{si_3}^n = \frac{3\varphi^{n+1} - 4\varphi^n + \varphi^{n-1}}{2\Delta t}.$$

We then proceed to update  $w^{n+1}$  with one of these values ( $\psi_{si_1}, \psi_{si_2}$  or  $\psi_{si_3}$ ).

In the third order case, we use a similar segregated strategy. We first compute an approximation of  $\zeta^{n+1}$  using the first order approximation  $\psi_{e_1}^n$  and  $w^n$  to evaluate the third order derivative. This value is used to estimate  $\varphi^{n+1}$  and used to compute  $\psi_{si}$  as before, and also to estimate

$$\theta_{si}^n = \frac{\varphi^{n+1} - 2\varphi^n + \varphi^{n-1}}{\Delta t^2}.$$

These values are used to evaluate  $w^{n+1}$  using Eq 5. In the non-linear case, Eq 3 shows a coupling between the value of  $\varphi^{n+1}$  and  $w^{n+1}$ . Replacing  $w^{n+1}$  with  $w^n$  introduces an  $\mathcal{O}(\Delta t)$  error we minimize performing sub-iterations of the scheme, re-evaluating both  $\zeta^{n+1}$  and  $w^{n+1}$  with the updated  $\psi$  and  $\varphi$  values.

The schemes obtained with the above approaches are in the following referred to as the LW2e<sub>1</sub>, LW2e<sub>2</sub>, LW2si<sub>1</sub>, and LW2si<sub>2</sub> and LW2si<sub>3</sub> in the second order case using the various definitions of the auxiliary variables. Similarly we denote by LW3<sub>e</sub> and LW3si the third order schemes obtained using respectively  $\psi_{e_2}$  and  $\theta_e$ , and  $\psi_{si_2}$  and  $\theta_{si}$ .

### 3.4 Simplified LW3 scheme via $\mathcal{O}(\Delta t^3, \mu^2 \Delta t^2)$ truncation

The previous approaches are based on neglecting  $\mathcal{O}(\Delta t^3)$  terms in the truncated Taylor series. Using arguments similar to those put forward in the previous section, we may use the smallness of  $\mu^2$  to simplify somewhat the scheme. In particular, we may choose to also neglect terms of  $\mathcal{O}(\mu^2 \Delta t^2)$  in the development. This leads to several possibilities, as we may choose to keep some of the truncation terms, and only neglect those adding a large computational effort. To this end, we consider the linear limit of the third order method, on a flat bathymetry, which we recast as:

$$\left\{ \begin{array}{l} \frac{\zeta^{n+1} - \zeta^n}{\Delta t} + \partial_x w^n = \frac{\Delta t}{2} \partial_{xx} \zeta^n - \frac{\mu^2 \Delta t}{2} \partial_x \varphi_1^n - \frac{\Delta t^2}{6} \partial_{xxx} w^n - \frac{\mu^2 \Delta t^2}{6} \partial_x \psi_1^n \\ \frac{w^{n+1} - w^n}{\Delta t} + \partial_x \zeta^n = \mu^2 \varphi_1^n + \frac{\Delta t}{2} \partial_{xx} w^n + \frac{\mu^2 \Delta t}{2} \psi_1^n - \frac{\Delta t^2}{6} \partial_{xxx} \zeta^n + \frac{\mu^2 \Delta t^2}{6} (\partial_{xx} \varphi_1^n + \theta_1^n) \\ \varphi_1^n - \mu^2 \alpha \partial_{xx} \varphi_1^n = -\gamma \partial_{xxx} \zeta^n \\ \psi_1^n - \mu^2 \alpha \partial_{xx} \psi_1^n = \gamma \partial_{xxxx} w^n \\ \theta_1^n - \mu^2 \alpha \partial_{xx} \theta_1^n = -\gamma \partial_{xxxx} \zeta^n + \mu^2 \gamma \partial_{xxxx} \varphi_1^n \end{array} \right.$$

having set  $\varphi = \mu^2 \varphi_1$ . We can now define different versions of a simplified LW3 method, depending on which of the  $\mu^2 \Delta t^2$  terms are neglected.

In particular, seven versions of simplified LW3 schemes are defined in Table 1 by neglecting some of the three  $\mu^2 \Delta t^2$  terms in equations :  $\frac{\mu^2 \Delta t^2}{6} \partial_x \psi_1$ ,  $\frac{\mu^2 \Delta t^2}{6} \partial_{xx} \varphi_1$  and  $\frac{\mu^2 \Delta t^2}{6} \theta_1$ . The objective of the next sections is to retain the most accurate and stable of these schemes. To this end, we will perform a spectral analysis to evaluate the dispersion and dissipation error of the schemes. As a preliminary step, we will evaluate which of the simplified LW3 formulas to retain.

## 4 Spectral properties of the time discretizations

In this Section, we analyze the spectral properties of the numerical schemes of Section 3 studying their dispersion relation's errors, solving for both the standard and the enhanced Boussinesq equations.

Terms	$\frac{\mu^2 \Delta t^2}{6} \partial_x \psi_1^n$	$\frac{\mu^2 \Delta t^2}{6} \partial_{xx} \varphi_1^n$	$\frac{\mu^2 \Delta t^2}{6} \theta_1^n$
Version 1	no	no	no
Version 2	no	yes	no
Version 3	yes	yes	no
Version 4	yes	no	no
Version 5	no	no	yes
Version 6	no	yes	yes
Version 7	yes	no	yes

Table 1: Simplified LW3 schemes. We note 'yes' when the term is present in the version proposed, and 'no' when it is removed.

The dispersion relations are determined assuming a flat bottom and a linear propagation in the positive direction.

We summarize the determination of the relation dispersion in three steps:

1. Denoting  $\nu = \omega + i\xi$ , we express each variable  $X$  of the system ( $\eta, u$  and  $\varphi$ ) in the form  $X_0 e^{i(2\pi x - \nu t)}$ , where  $X_0$  is a constant. Here,  $\omega$  and  $\xi$  may be considered as parameters of dispersion and amplification, respectively.
2. We formally replace  $\nu$  by its expression and separate the equations for real and imaginary parts.
3. From this new system, we can then determine  $\omega$  and  $\xi$ .

This analysis is of course performed for the linear version of the scheme [20], which we report in Annex A for completeness.

To evaluate the schemes, we will compare the discrete dispersion relations with those of the Airy equations [8], and with the exact dispersion relation of the standard and enhanced Boussinesq equations. These are reported in the Annex B. We evaluate the influence of the time step and of the frequential dispersion parameter on the accuracy of the schemes for a range of 50 values of  $kd$  between 0 and 4.

We also denote  $Nc = 1/\Delta t$  ( $\Delta t$  is the dimensionless time step) the number of time steps needed for a wave to propagate over a wavelength at the celerity  $c$ . The discrete dispersion relations are also reported in Annex B for completeness.

The Runge-Kutta and full Lax-Wendroff schemes of same order define the same dispersion relation. As a consequence, only the Runge-Kutta results appear in the figures and tables.

#### 4.1 Preliminary study of the simplified LW3 versions

As a preliminary step, we investigate the spectral properties of the different versions of the simplified LW3 presented in Table 1.

Fig 2 and Fig 3 show the a) dispersion and b) diffusion errors in the dispersion relations of the seven simplified LW3 schemes solving the standard and enhanced Boussinesq equations, respectively. Fig 2 and Fig 3 show that the version without  $\frac{\mu^2 \Delta t^2}{6} \theta_1$  (version 3 in Table 1) produces better results. As regards enhanced Boussinesq Equations, only the simplified LW3 scheme version 3 produces better results than the explicit Euler scheme for all the range of  $kd$  values. As regards standard

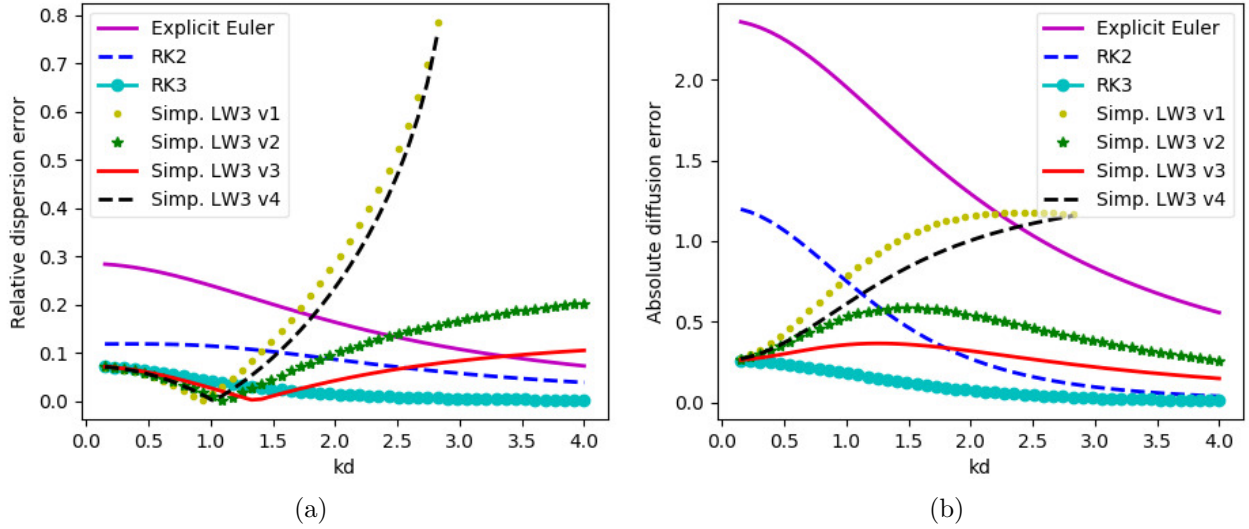


Figure 2: Error in the 2a) dispersion and 2b) diffusion calculated using schemes solving the standard Boussinesq equations with  $N_c = 5$ , compared to the standard Boussinesq equations' dispersion relation. While plotting the different simplified LW3 curves, we highlight that keeping or erasing the term in  $\theta_1$  does not change the curves, thus we plot only four simplified LW3 schemes.

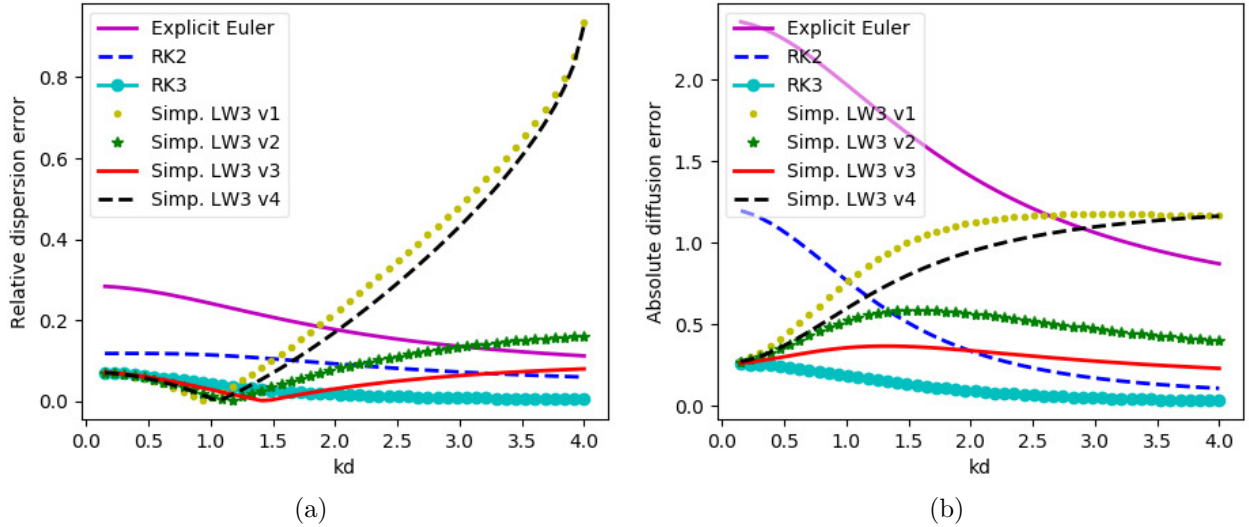


Figure 3: Error in the 3a) dispersion and 3b) diffusion calculated using schemes solving the enhanced Boussinesq equations with  $N_c = 5$ , compared to the standard Boussinesq equations' dispersion relation. While plotting the different simplified LW3 curves, we highlight that keeping or erasing the term in  $\theta_1$  does not change the curves, thus we plot only four simplified LW3 schemes.

Boussinesq equations, this version produces more accurate results than the explicit Euler scheme for most of  $kd$  values, but not for the shorter waves. Version 3 (without term including  $\theta_1$ ) is selected in the paper and is referred to hereafter as the "simplified LW3 scheme".

As regards the calculation of  $\psi_1$  in the simplified LW3 scheme, any attempt to replace the inversion of matrix used to calculate  $\psi_1$  (Eq 14 in Annex A) produces poor results. These finite difference discretizations (of order up to the fourth) result in schemes which are more dispersive than the Explicit Euler scheme for short waves. To conclude this preliminary study, we will only consider in the following the version 3 of the simplified LW3 method, and keep the inversion of the matrix (Eq 14).

## 4.2 Spectral analysis of the schemes for the standard Boussinesq equations

Compared to the enhanced Boussinesq equations, standard Boussinesq equations coarsely approximate the Airy equations. As already said, these equations can be obtained from Eqs 1,2 and 3 by setting  $\alpha = 1/3$  and  $\beta = 0$ .

Numerical schemes are compared, firstly to Airy equations (Table 2 and 3), then to exact standard Boussinesq equations (Fig 4 and 5). All the dispersion relations are presented in Annex B.

Scheme	$Nc = 5$	$Nc = 10$	$Nc = 20$	$Nc = 40$
Explicit Euler	0.24	0.12	0.09	0.08
RK2	0.10	0.08	0.08	0.08
LW2e <sub>1</sub>	0.13	0.09	0.08	0.08
LW2e <sub>2</sub>	0.10	0.08	0.08	0.08
LW2si <sub>1</sub>	0.10	0.06	0.07	0.08
LW2si <sub>2</sub>	0.10	0.08	0.08	0.08
LW2si <sub>3</sub>	0.11	0.06	0.07	0.07
RK3	0.08	0.08	0.08	0.08
LW3e	0.11	0.08	0.08	0.08
LW3si	0.08	0.08	0.08	0.08
Simp. LW3 v3	0.12	0.09	0.08	0.08

Table 2: Relative error of  $\omega$  calculated solving the standard Boussinesq equations in  $L^2$  norm compared to the exact solution of the Airy equations. We note  $Nc = 1/\Delta t$ .

Numerical dispersion error of schemes for  $Nc = 5, 10, 20$  and  $40$  is evaluated by analyzing  $\omega$  for  $kd$  values in the range  $[0,4]$  (Table 2). We consider in the spectral analysis an  $L^2$  error defined as :

$$err_{L^2} f(kd) = \frac{\sqrt{\sum_{i=1}^{50} (f_i - f_{ex}(k_i d))^2}}{\sqrt{\sum_{i=1}^{50} (f_{ex}(k_i d))^2}}$$

As shown in Table 2, we observe a certain error reduction when increasing the number of points. The residual error with reference to the Airy theory is about 7% and is attributed to the Boussinesq approximation. For small values of  $Nc$ , the simplified LW3 scheme, the LW2e<sub>1</sub> and the Explicit Euler schemes are the least accurate and the error of the Explicit Euler scheme is up to twice or

thrice larger than the ones of other schemes. For large values of  $Nc$ , all schemes converge to an error of about 7%. The LW2si<sub>3</sub> and LW2si<sub>1</sub> schemes converge slightly quicker than the other schemes.

Scheme	$Nc = 5$	$Nc = 10$	$Nc = 20$	$Nc = 40$
Explicit Euler	10.43	6.81	3.74	1.92
RK2	3.94	0.59	0.07	0.01
LW2e <sub>1</sub>	3.19	0.49	0.06	0.01
LW2e <sub>2</sub>	3.67	0.69	0.09	0.01
LW2si <sub>1</sub>	5.05	0.75	0.10	0.01
LW2si <sub>2</sub>	3.78	0.58	0.07	0.01
LW2si <sub>3</sub>	7.11	1.02	0.12	0.02
RK3	0.92	0.18	0.02	0.00
LW3e	0.99	0.16	0.02	0.00
LW3si	1.36	0.23	0.03	0.00
Simp. LW3 v3	2.01	0.30	0.04	0.01

Table 3: Absolute error of  $\xi$  in  $L^2$  norm obtained solving the standard Boussinesq equations. For both Airy and Boussinesq equations, the exact solution does not create diffusion ( $\xi = 0$ ).

Numerical diffusion error of schemes for  $Nc = 5, 10, 20$  and  $40$  is evaluated by analyzing  $\omega$  in the same range of  $kd$  values (Table 3). As shown in Table 3, all the schemes converge in time to a null diffusion. The first order Explicit Euler scheme is the most diffusive. Among the second-order schemes, the LW2si<sub>3</sub> scheme is the most diffusive and the LW2e<sub>1</sub> scheme is the less diffusive scheme. The most diffusive third-order scheme is the LW3si scheme. The least diffusive ones are the RK3 and LW3e schemes.

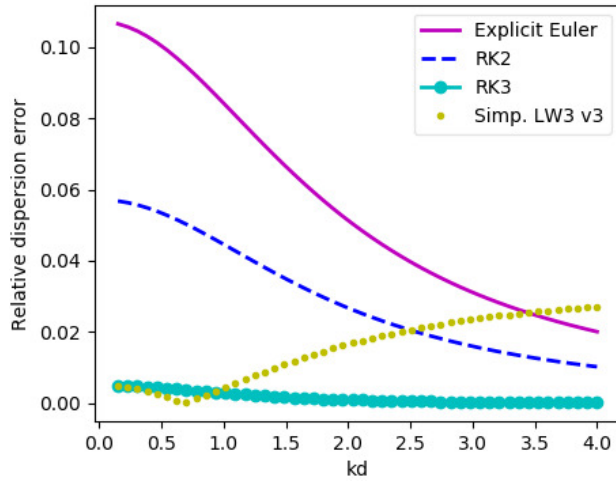
In addition to Tables 2 and 3, Fig 4 and 5 illustrate the influence of  $kd$  on the dispersion and diffusion errors.

In Fig 4, numerical dispersion of schemes for  $Nc = 10$  is further evaluated by analyzing  $\omega$  as a function of  $kd$ . While the simplified-third order scheme is more accurate for small  $kd$  than for great  $kd$ , the Runge-Kutta and Explicit Euler schemes have an opposite behaviour. Surprisingly, the curves corresponding to the LW2e<sub>1</sub>, LW3e and simplified LW3 schemes have points of inflexion. Across these values, the schemes go from an underestimation to an overestimation of celerities, compared to the analytical solution. Concerning the second-order schemes, RK2 and LW2si<sub>2</sub> (where the second matrix inversion is replaced by FD temporal derivatives of  $\varphi$ ) produce the same results.

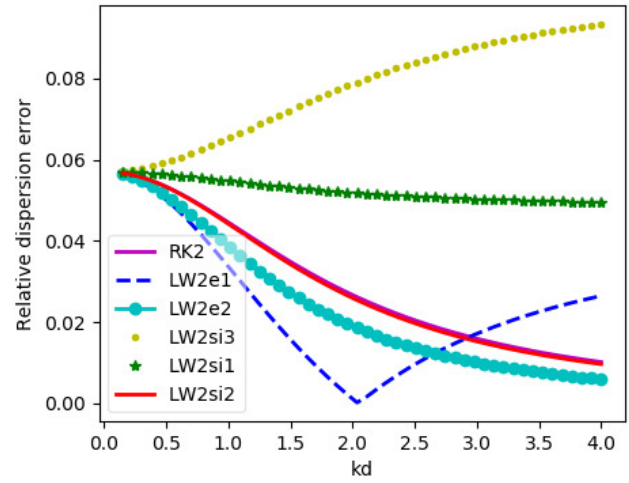
Similarly to the phase error, the numerical diffusion of the schemes for  $Nc = 10$  is further evaluated in Fig 5 by analyzing  $\xi$  as a function of  $kd$ . As in Fig 4, not all schemes provide a monotone behaviour. In particular, some show a change in the sign of the amplification rate, which however tends to zero for all schemes as  $kd$  increases. The Explicit Euler one is far more diffusive than the other schemes. In terms of diffusion, the results of the LW2si<sub>2</sub> scheme are close to those obtained by the RK2 dispersion relation.

In summary, solving the standard Boussinesq equations, the spectral analysis shows that :

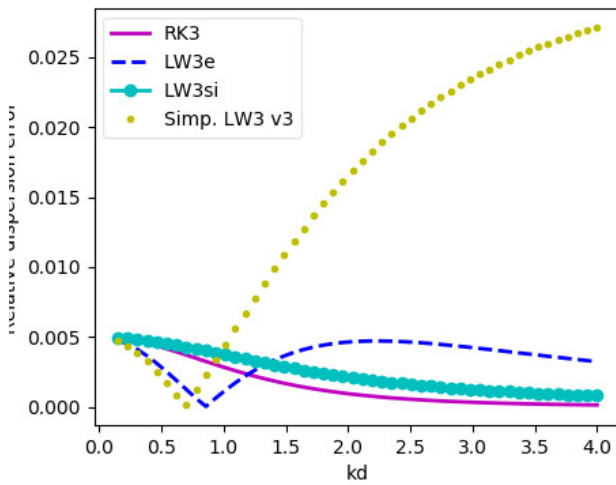
- The explicit Euler scheme produces the worst results in terms of dispersion and diffusion results.
- The implicit forward LW2si<sub>3</sub> and LW2si<sub>1</sub> schemes are two of the most diffusive schemes. Despite their good accuracy in dispersion compared to the Airy equations, they generate poor



(a)

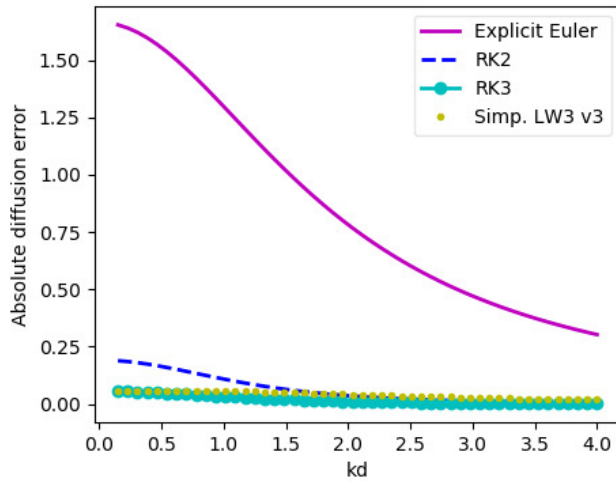


(b)

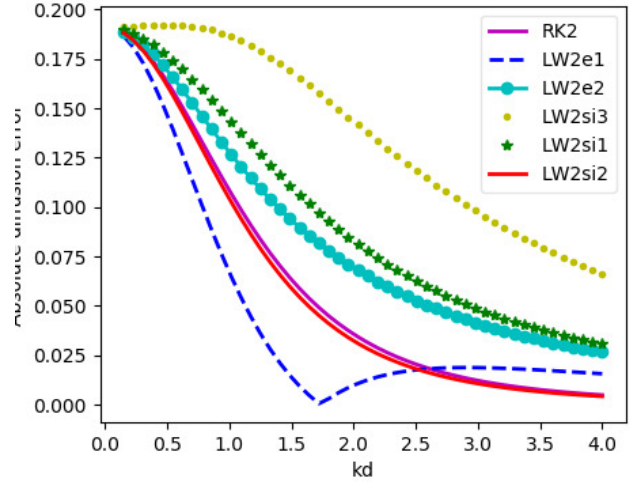


(c)

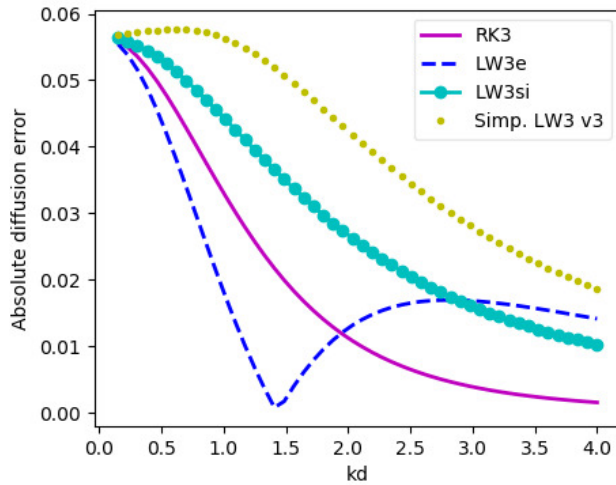
Figure 4: Error in the dispersion calculated using 4a) explicit Euler, RK2, RK3 and simplified LW3 schemes, 4b) second-order schemes, 4c) third-order and simplified LW3 schemes, solving the standard Boussinesq equations with  $Nc = 10$ , compared to the exact dispersion relation of the standard Boussinesq equations. The curves corresponding to the RK2 and LW2si<sub>2</sub> schemes are identical.



(a)



(b)



(c)

Figure 5: Error in the diffusion calculated using 5a) Explicit Euler, RK2, RK3 and simplified LW3 schemes, 5b) second-order schemes, 5c) third-order and simplified LW3 schemes, solving the standard Boussinesq equations with  $Nc = 10$ . The curves corresponding to the RK2 and LW2si<sub>2</sub> schemes are nearly totally identical.

results compared to the Boussinesq equations. We attribute this difference to the numerical error, which tends to bring the numerical results nearer to the Airy results.

- LW2 and RK2 schemes generate identical results, since their dispersion relations are the same.
- The implicit centered LW2si<sub>2</sub> scheme produces similar results to the LW2 and RK2 schemes.
- Results of third-order schemes are close to each other in terms of dispersion and diffusion. These schemes converge faster to the solution than the second order schemes.
- The simplified third-order scheme, which has diffusion properties similar to the third-order schemes, generates a dispersion error similar to the third-order schemes for long waves and to the second-order schemes for short waves.

### 4.3 Solving Enhanced Boussinesq Equations

Dispersion and diffusion errors of schemes are calculated in this section for the enhanced Boussinesq equations. These equations approximate more closely the Airy equations.

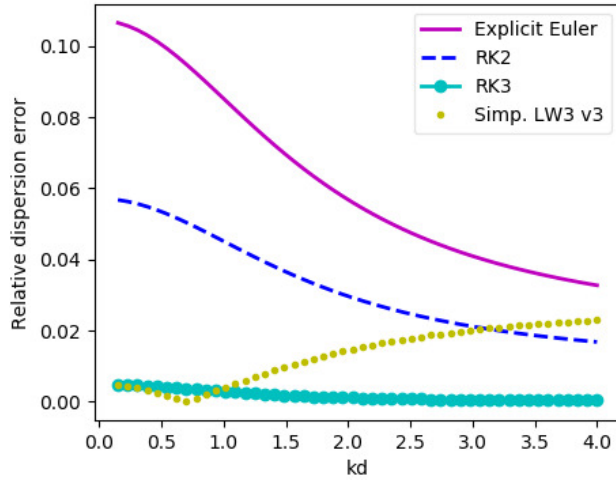
Scheme	$Nc = 5$	$Nc = 10$	$Nc = 20$	$Nc = 40$
Explicit Euler	0.22	0.08	0.02	0.01
RK2	0.10	0.04	0.01	0.01
LW2e <sub>1</sub>	0.08	0.03	0.01	0.01
LW2e <sub>2</sub>	0.07	0.04	0.01	0.01
LW2si <sub>1</sub>	0.14	0.06	0.02	0.01
LW2si <sub>2</sub>	0.11	0.04	0.01	0.01
LW2si <sub>3</sub>	0.16	0.07	0.02	0.01
RK3	0.04	0.01	0.01	0.01
LW3e	0.04	0.01	0.01	0.01
LW3si	0.05	0.01	0.01	0.01
Simp. LW3 v3	0.05	0.01	0.01	0.01

Table 4: Relative error of  $\omega$  calculated by solving the enhanced Boussinesq equations in  $L^2$  norm compared to the exact solution of the Airy equations. We denote  $Nc = 1/\Delta t$ .

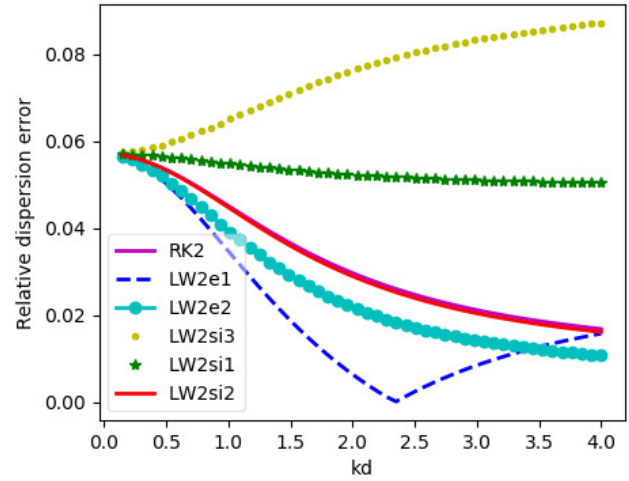
As before, we compute the numerical dispersion error of the schemes for  $Nc = 5, 10, 20$  and  $40$  in the range  $[0,4]$  of  $kd$  values. The results in Table 4 show that all schemes converge to the Airy equations dispersion relation with an error less than 1%. The Explicit Euler, LW2si<sub>3</sub> and LW2si<sub>1</sub> show the slowest reduction in error and can be considered as less accurate. On the other hand, all the third order formulations, including the simplified one, quickly provide a discretization error below the truncation of the model.

The amplification rates for  $Nc = 5, 10, 20$  and  $40$  are evaluated by analyzing  $\omega$  in the same range of  $kd$  values (Table 5). Conclusions are identical to the ones obtained solving the standard Boussinesq equations in Section 4.2.

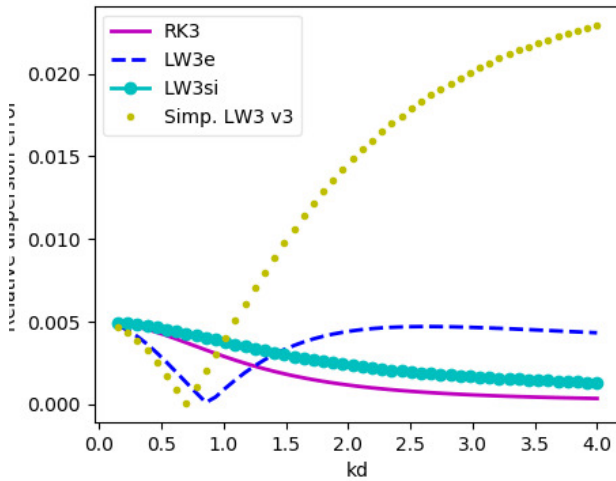
Dispersion and diffusion errors are presented for  $Nc = 10$  in Fig 6 and Fig 7, respectively. As before, we observe a change of sign in the phase error of the LW2e<sub>1</sub>, LW3e and simplified scheme. Schemes without change of sign are accurate with an error monotonically tending to zero as the frequential dispersion reduces. The exception is the LW2si<sub>3</sub> which provides a dispersion error



(a)



(b)



(c)

Figure 6: Dispersion error calculated for 6a) explicit Euler, RK2, RK3 and simplified LW3 schemes, 6b) second-order schemes, 6c) third-order and simplified LW3 schemes solving the enhanced Boussinesq equations with  $N_c = 10$ , compared to the enhanced Boussinesq equations' dispersion relation. The curves of the RK2 and LW2si<sub>2</sub> schemes are identical.

Scheme	$Nc = 5$	$Nc = 10$	$Nc = 20$	$Nc = 40$
Explicit Euler	11.07	7.21	3.95	2.03
RK2	4.08	0.61	0.08	0.01
LW2e <sub>1</sub>	3.23	0.49	0.06	0.01
LW2e <sub>2</sub>	3.79	0.72	0.10	0.01
LW2si <sub>1</sub>	5.35	0.80	0.10	0.01
LW2si <sub>2</sub>	3.90	0.59	0.08	0.01
LW2si <sub>3</sub>	7.50	1.09	0.13	0.02
RK3	0.96	0.18	0.02	0.00
LW3e	1.00	0.16	0.02	0.00
LW3si	1.46	0.25	0.03	0.00
Simp. LW3 v3	2.17	0.32	0.04	0.01

Table 5: Absolute error of  $\xi$  in  $L^2$  norm obtained by solving the enhanced Boussinesq equations. For the Airy and Boussinesq equations, the exact solution does not create diffusion, so we look for errors around zero.

increasing with  $kd$ . As in the case of the standard Boussinesq equations, the RK2 and LW2si<sub>2</sub> schemes give the same results.

With regards to diffusion, results (Fig 7) confirm that the Explicit Euler scheme is the most diffusive scheme and that RK2 and LW2si<sub>2</sub> schemes produce similar results.

In summary, this study of the schemes solving the enhanced Boussinesq equations shows that :

- While solving the enhanced Boussinesq equations, the LW2si<sub>3</sub> and LW2si<sub>1</sub> schemes are the least accurate compared to Airy equations' dispersion relation.
- The third order schemes generally provide improved spectral accuracy. Among them, the LW3si and LW3e seem to be the most promising simplified formulations.

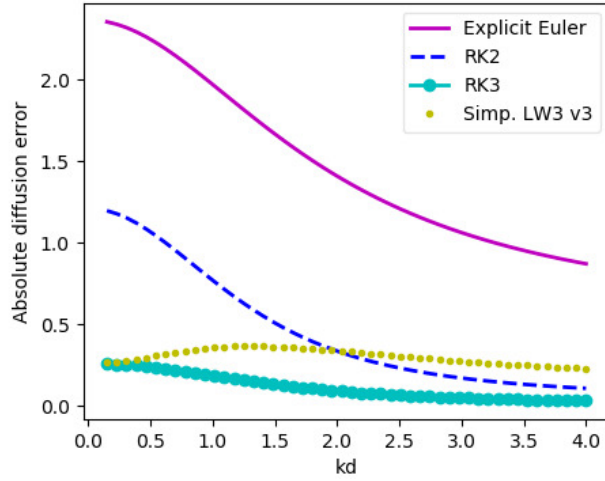
As a result of these observations, we will not consider further the explicit Euler, the LW2si<sub>1</sub> and the LW2si<sub>3</sub> schemes.

## 5 Numerical tests

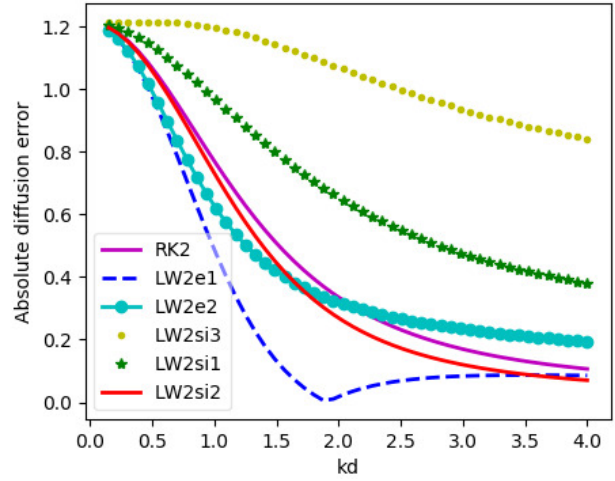
This section is devoted to the simulation of four benchmarks to evaluate the accuracy and computational cost of the schemes under study.

For all benchmarks, we use a constant time step calculated from a CFL condition. This condition is defined by  $c\Delta t < CFL \Delta x$  where  $c$  is the celerity based on the average initial depth and  $\Delta x$  the space step. This type of setting is not uncommon in tsunami analysis and CFL is set by default to 0.5 in this paper.

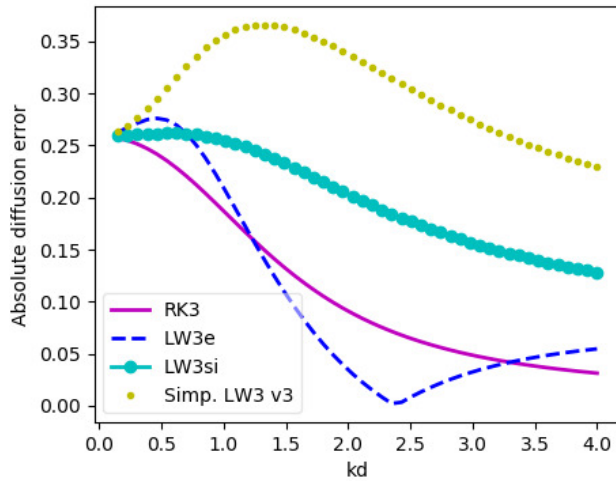
In the figures, all results are made non-dimensional. For the undular bore (Section 5.3), it is made dividing the dimensional values by  $d_0$ . For the other benchmarks, it is made as discussed in section 2. We note  $n$  the number of points in the discretized domain and use as values of  $d_0$  and  $a_0$  the mean of  $\eta'$  and  $d'$  respectively. All results are compared to a high-resolution numerical solution calculated by a RK3 scheme.



(a)



(b)



(c)

Figure 7: Diffusion error calculated for 7a) explicit Euler, RK2, RK3 and simplified LW3 schemes, 7b) second-order schemes, 7c) third-order and simplified LW3 schemes solving the enhanced Boussinesq equations with  $Nc = 5$ , compared to the exact Airy equations' dispersion relation.

## 5.1 Gaussian wave

The first benchmark consists in simulating the propagation of a gaussian wave with an amplitude of 10 cm and a standard deviation of 60 m over a distance of 24,000 m. The water depth is 10 m, the initial velocity is null and the characteristic wavelength is  $l = 250$  m.

This benchmark is characterized by a linear propagation of strongly dispersive waves. In order to generate significant differences between the schemes, a large space step has been selected ( $n = 2001$ ), so that the initial wave is described by about 10 points. We compare the results to a high-resolution computed solution (or reference solution) calculated by the RK3 scheme with 8004 points ( $\Delta x \simeq 3$  m) and  $CFL = 0.5$ .

Fig 8 shows the water surface calculated by the second and third-order schemes at  $t = 17.43$  and  $t = 34.86$ . The results show that the resolution of the secondary waves gets worse as their distance from the main front increases. We also see that the second order schemes produce increasing wave amplitudes, which is a sign of a numerical instability. These schemes also introduce large numerical dispersion which results in increasing time advance of the wave train compared to the reference solution.

By contrast, the third order schemes are stable and generate a wave train with progressively decreasing amplitudes. For all third-order schemes, this decrease is stronger than in the reference solution, which is a consequence of the damping of the schemes. The phase error is much reduced, and is relatively small up to the fourth or fifth peak from the main wave.

The same simulations are performed by dividing by two the space step ( $n = 4001$ ) while keeping the CFL equal to 0.5 (Fig 9). The third order schemes give results very close to the reference solution for roughly 10 peaks, and then show a slight dumping with a small phase error, still much smaller than that of the second order methods.

Scheme	n = 1001	n = 2001	n = 3001	n = 4002	n = 5002	n = 6003
RK2	1.89	1.82	1.54	1.24	0.91	0.69
LW2e <sub>1</sub>	1.75	1.78	1.45	1.14	0.81	0.61
LW2e <sub>2</sub>	2.00	2.32	1.73	1.30	0.93	0.69
LW2si <sub>2</sub>	1.89	1.82	1.54	1.24	0.91	0.69
LW2	1.94	1.95	1.57	1.25	0.91	0.69
RK3	0.83	0.70	0.53	0.18	0.10	0.04
LW3e	0.84	0.71	0.56	0.19	0.10	0.04
LW3si	0.83	0.69	0.52	0.18	0.10	0.05
LW3	0.83	0.70	0.53	0.18	0.10	0.04
Simp. LW3 v3	0.83	0.71	0.59	0.26	0.16	0.08

Table 6: Relative error (in  $L^2$  norm) of the water height calculated in simulations of the propagation of the gaussian wave through the enhanced Boussinesq equations, for six different space steps ( $n = 1001, 2001, 3001, 4002, 5002, 6003$ ). We keep the CFL parameter to 0.5. The errors are obtained comparing the numerical results to those obtained applying RK3 with  $n = 8004$  and  $CFL = 0.5$ .

We further investigate the errors (Table 6) and the computational times (Table 7) for six values of space steps ( $n = 1001, 2001, 3001, 4002, 5002, 6003$ ). Concerning the second order schemes, Table 6 and Table 7 show that the LW2e<sub>1</sub> is the least CPU-expensive scheme and the most accurate one. Among the third order schemes, all the formulations considered give results with similar accuracy but, as expected, the CPU-time of the simplified scheme is about 6% lower than the LW3 CPU-time,

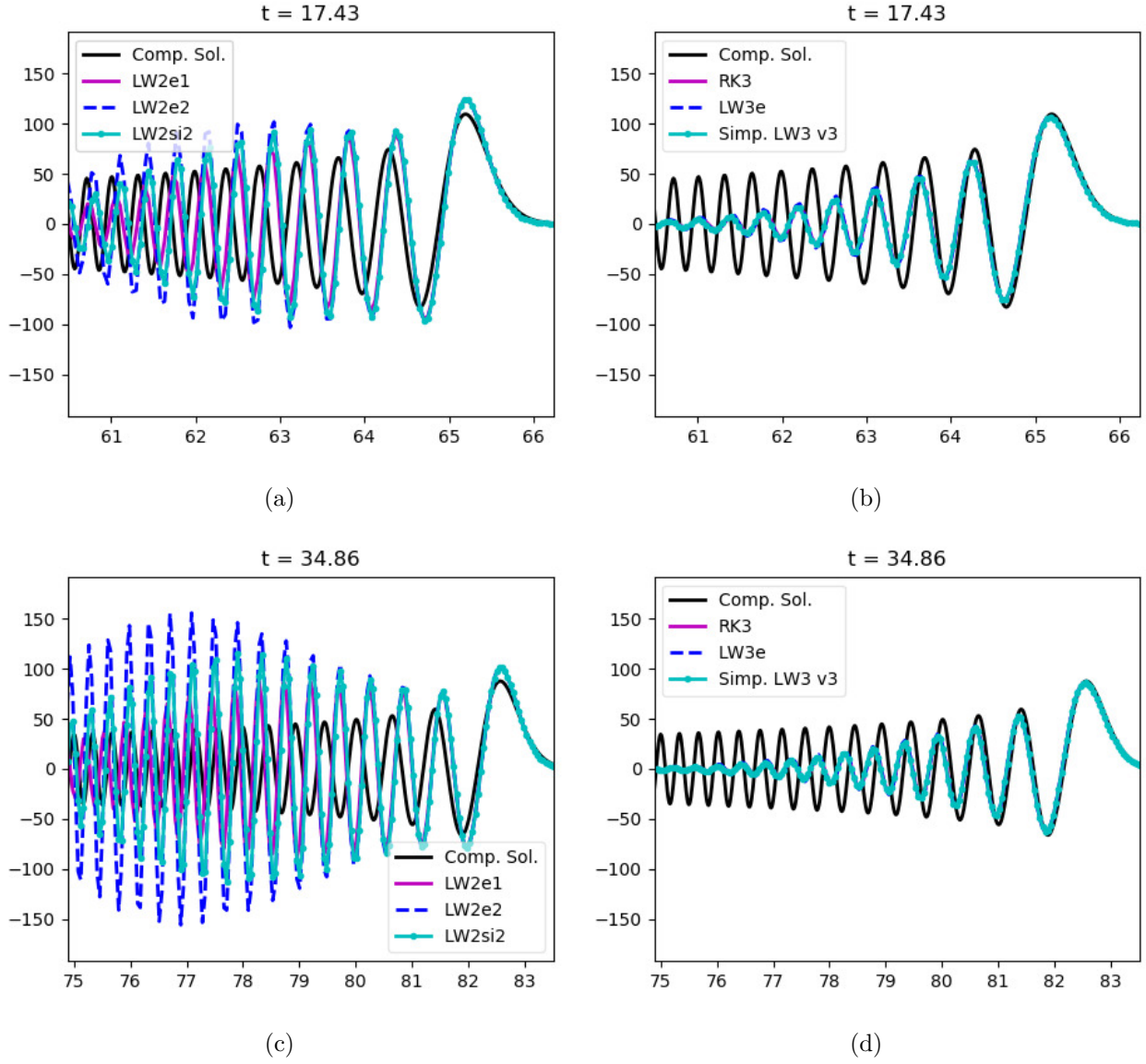


Figure 8: Propagation of a gaussian wave simulated with  $n = 2001$  by 8a,8c) LW2e<sub>1</sub>, LW2e<sub>2</sub> and LW2si<sub>2</sub> schemes, 8b,8d) third-order and simplified LW3 schemes. The enhanced nonlinear Boussinesq equations are solved at 8a,8b)  $t = 17.43$  (top) and 8c,8d)  $t = 34.86$  (bottom). Comp. Sol. denotes the reference solution obtained applying RK3 with  $n = 8004$  and  $CFL = 0.5$ . RK2 and LW2 results are close to the LW2si<sub>2</sub> ones and then are not plotted. The same applies to LW3 and LW3si schemes since their results are nearly identical to the RK3 ones. Values on x-axis and y-axis are expressed in dimensionless form.

and about 30% lower than the RK3 CPU-time. The least expensive third-order scheme for a given error level is the explicit LW3e.

The  $L^2$  error and the CPU-time are plotted in Fig 10 for the six spatial resolutions. Results show that all the schemes of same order converge with the expected second and third order rates.

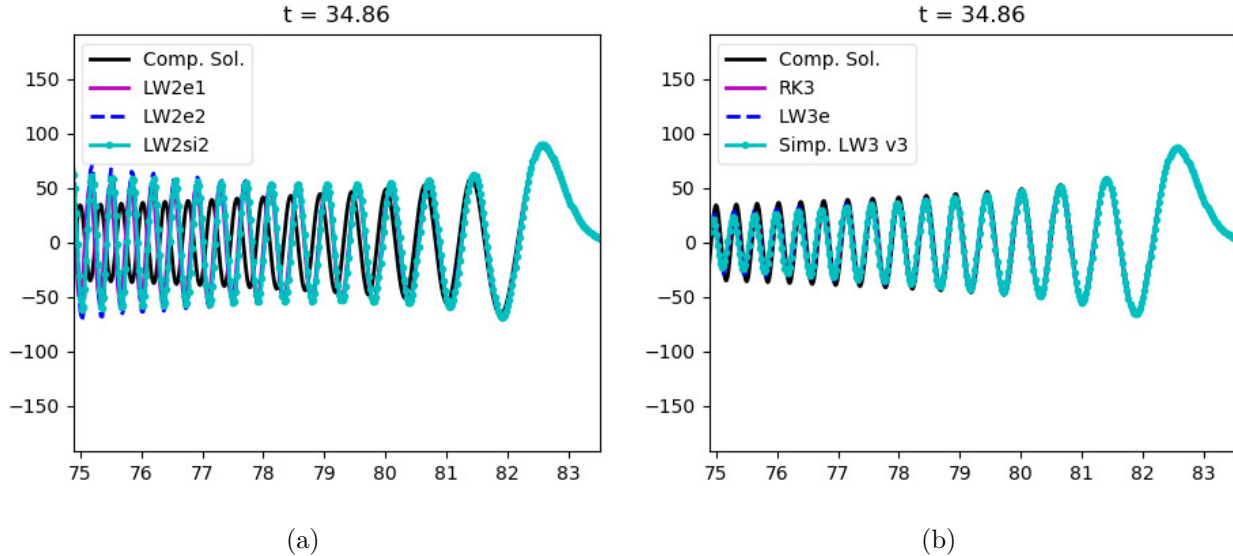
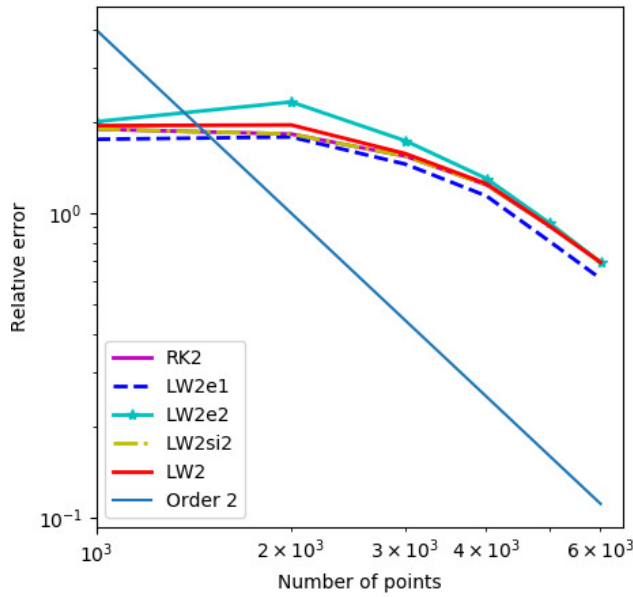


Figure 9: Propagation of a gaussian wave simulated with  $n = 4001$  by 9a) LW2e<sub>1</sub>, LW2e<sub>2</sub> and LW2si<sub>2</sub> schemes, 9b) third-order and simplified LW3 schemes solving the enhanced nonlinear Boussinesq equations. Comp. Sol. denotes the reference solution obtained applying RK3 with  $n = 8004$  and  $CFL = 0.5$ . The curves corresponding to the LW2si<sub>2</sub>, LW2e<sub>1</sub> and LW2e<sub>2</sub> schemes are identical. The curves corresponding to the RK2, LW3e and simplified LW3 schemes are identical. Values on x-axis and y-axis are expressed in dimensionless form.

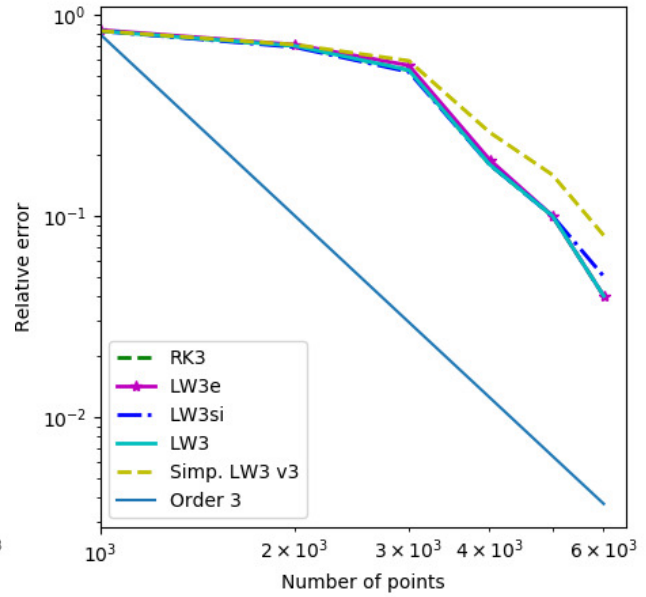
Scheme	$n = 1001$	$n = 2001$	$n = 3001$	$n = 4002$	$n = 5002$	$n = 6003$
RK2	7	52	176	389	799	1731
LW2e <sub>1</sub>	4	31	105	232	499	901
LW2e <sub>2</sub>	4	31	98	251	492	1002
LW2si <sub>2</sub>	6	48	145	402	762	1440
LW2	6	45	132	339	691	1385
RK3	10	77	260	602	1120	2322
LW3e	6	49	146	380	719	1328
LW3si	11	88	261	681	1298	2400
LW3	9	70	204	528	1043	2100
Simp. LW3 v3	7	56	161	434	821	1630

Table 7: Computational time (in seconds) of the schemes solving the enhanced Boussinesq equations to simulate the propagation of a gaussian wave, for six different values of the space step ( $n = 1001, 2001, 3001, 4002, 5002, 6003$ ). We keep the CFL parameter to 0.5.

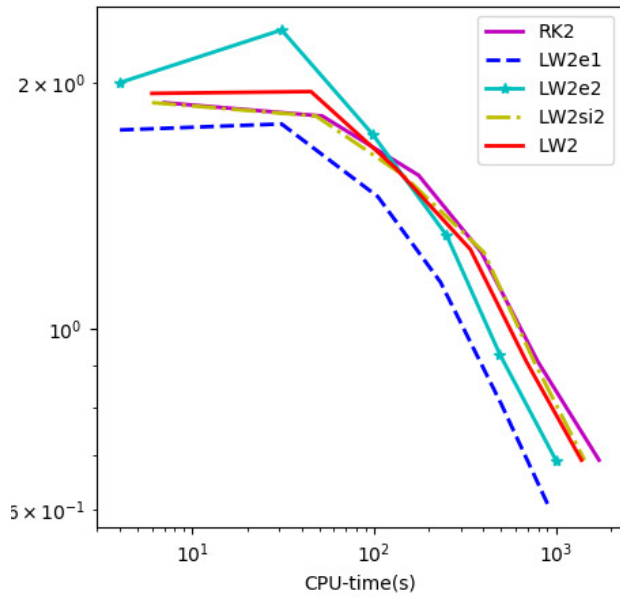
The LW2e<sub>1</sub> scheme converges faster than the other second-order schemes. As one may expect, the convergence rate of the simplified LW3 scheme, in which some of the terms in the Taylor series in time are missing, is slightly below 3. Results also show that for a given accuracy, the LW2e<sub>1</sub> and LW3e schemes are faster than the other second-order and third-order schemes, respectively.



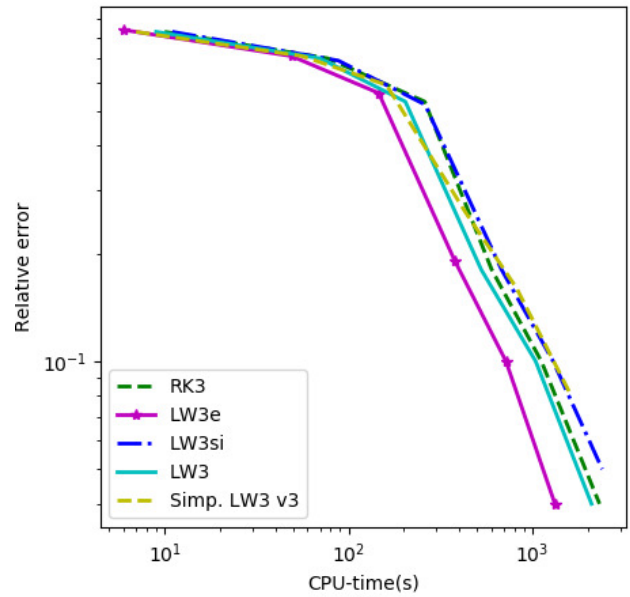
(a)



(b)



(c)



(d)

Figure 10: Relative error (in  $L^2$  norm) of the water height calculated in simulations of the propagation of the gaussian wave for  $n = 1001, 2001, 3001, 4002, 5002, 6003$ . The results are obtained solving the enhanced Boussinesq equations by 10a,10c) second-order schemes, 10b,10d) third-order and simplified LW3 schemes. The results are compared to a high-resolution computed solution and their error is expressed depending on 10a,10b) the number of points of discretization, 10c,10d) the CPU-time . The computational solution is obtained applying RK3 with  $n = 8004$  and  $CFL = 0.5$ . Curves are plotted in logarithmic scale.

## 5.2 Solitary wave

The second benchmark consists in the propagation in the positive direction of a solitary wave 2 m high centered at  $x_{mean} = 1000$  m over a 10 m deep bottom in a 5000 m long domain. The space step is 10 m (which corresponds to 501 points) and the characteristic wavelength is  $l = 400$  m.

The solitary wave is described by the approximate formulas:

$$\begin{aligned}\eta &= a[\operatorname{sech}(C(x - x_{mean}))]^2 \\ u &= \frac{c \times \eta}{\eta + d}\end{aligned}$$

where  $a$  is the maximum amplitude of the wave,  $x_{mean}$  is the position of the wave center,  $C = \sqrt{\frac{3a}{4(d+a)d^2}}$  and  $c = \sqrt{9.81(d+a)}$ . Note that this solitary wave is not an exact solution of the enhanced Boussinesq equations. However the error is expected to be of the order of the truncation of the model.

With this case, we check and evaluate the discretization of nonlinear terms. We remind that their absence results in the formation of a wave train. Reference solution is produced using the RK3 scheme in a mesh of 3000 points ( $\Delta x \simeq 1.6$  m) and a CFL of 0.49.

Fig 11 shows a comparison between the computed solution and results calculated by the second and third-order schemes at  $t = 10.89$  for two different spatial resolutions ( $n = 501, 1001$ ). This figure shows that the schemes of same order generate similar results and that the simplified LW3 scheme produces similar results to the third order ones. For coarse resolutions, the second order schemes (Fig 11a, 11c) overestimate the height of the wave and the other schemes (Fig 11b, 11d) underestimate it. Among the second-order schemes, the LW2e<sub>1</sub> scheme generates the most accurate results and the LW2e<sub>2</sub> scheme the worst ones.

Scheme	n = 250	n = 501	n = 1002	n = 1503	n = 2004	n = 2505
RK2	0.99	0.88	0.57	0.20	0.11	0.08
LW2e <sub>1</sub>	0.88	0.71	0.45	0.16	0.09	0.07
LW2e <sub>2</sub>	0.88	1.22	0.63	0.21	0.11	0.08
LW2si <sub>2</sub>	0.90	0.92	0.57	0.20	0.11	0.08
LW2	1.03	0.91	0.57	0.19	0.10	0.08
RK3	1.22	1.06	0.32	0.12	0.05	0.02
LW3e	1.22	1.04	0.27	0.10	0.04	0.02
LW3si	1.22	1.06	0.33	0.13	0.05	0.02
LW3	1.22	1.06	0.31	0.12	0.05	0.02
Simp. LW3 v3	1.22	1.06	0.34	0.14	0.06	0.03

Table 8: Relative error (in  $L^2$  norm) of the water height calculated in the simulations of the propagation of a solitary wave, solving the enhanced Boussinesq equations for six different values of the space step. We keep the CFL parameter to 0.5. The results are compared to the ones obtained applying RK3 with  $n = 3000$  and  $CFL = 0.9$ .

Relative error of schemes is studied in Table 8. Amongst the second-order schemes, the LW2e<sub>1</sub> is the most accurate and the LW2e<sub>2</sub> is the less accurate one. The third-order and simplified third-order schemes have similar accuracy, the LW3e scheme being slightly more accurate and the simplified LW3 scheme slightly less accurate than the others.

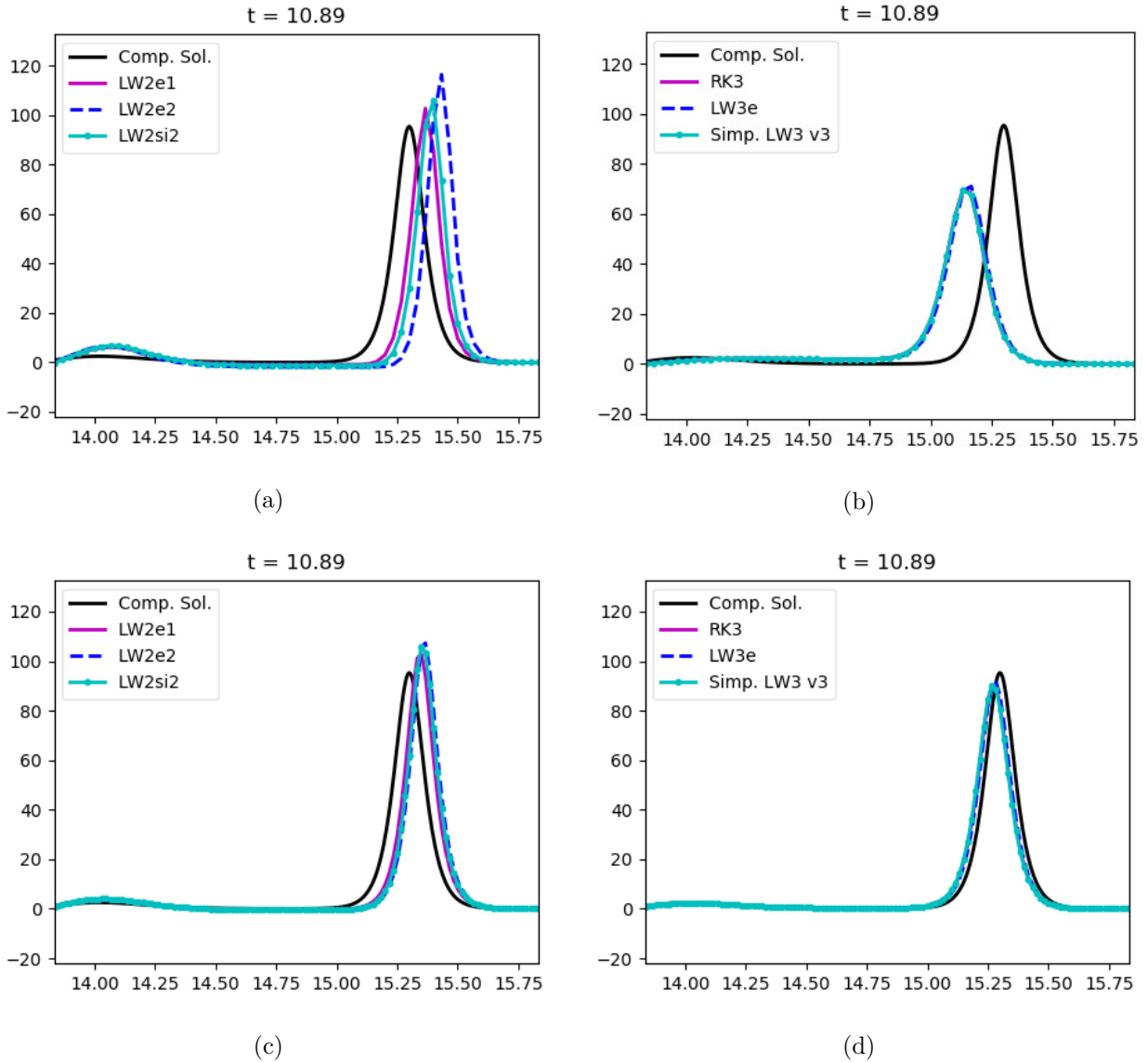


Figure 11: Propagation of a solitary wave simulated by 11a,11c) second-order schemes 11b,11d) third-order and simplified LW3 schemes solving the nonlinear enhanced Boussinesq equations. The equations are solved with 11a,11b)  $n = 501$  and 11c,11d)  $n = 1001$ . Values on x-axis and y-axis are expressed in dimensionless unities. Comp. Sol. denotes the reference solution obtained applying RK3 with  $n = 3000$  and  $CFL = 0.49$ . RK2 and LW2 results are similar to the LW2si<sub>2</sub> ones and then are not plotted. In the same way, LW3 and LW3si results are similar to the RK3 ones and are not plotted. The curves of the RK3 and simplified LW3 schemes are identical.

The CPU-time corresponding to the different schemes is provided in Table 9. As expected, the explicit LW2<sub>e1</sub>, LW2<sub>e2</sub> and LW3<sub>e</sub> schemes are the fastest ones, compared to the schemes of same order. The simplified LW3 scheme is slightly slower than the explicit LW3<sub>e</sub> scheme, and faster than the other third-order schemes. The Runge-Kutta and implicit LW2si<sub>2</sub> and LW3si schemes are the

Scheme	n = 250	n = 501	n = 1002	n = 1503	n = 2004	n = 2505
RK2	0.1	0.9	11.7	39.9	96.7	183.0
LW2e <sub>1</sub>	0.1	0.5	6.2	23.6	56.7	97.6
LW2e <sub>2</sub>	0.0	0.4	6.2	23.6	56.9	97.8
LW2si <sub>2</sub>	0.1	0.6	10.3	36.4	88.2	151.4
LW2	0.1	0.9	9.7	32.6	82.1	142.1
RK3	0.1	1.3	17.6	59.6	140.7	254.6
LW3e	0.1	0.6	10.1	37.6	90.4	154.3
LW3si	0.1	1.2	18.6	65.6	158.8	273.7
LW3	0.1	1.5	15.9	50.6	119.5	222.2
Simp. LW3 v3	0.1	1.0	11.9	40.1	85.8	174.3

Table 9: Computational time (in seconds) of the schemes simulating the propagation of a solitary wave for six different space steps. We keep the CFL parameter to 0.5.

slowest ones, compared to the schemes of same order. While being less accurate than the schemes of higher order, the RK2 and LW2si<sub>2</sub> schemes have a CPU-time similar or greater than the LW3e and simplified LW3 schemes, which highlights their computational cost. As in the linear benchmark of the gaussian wave, the LW3si and RK3 schemes are far more expensive than the LW3e and simplified LW3 schemes, and show no notable improvement of accuracy. In particular, the CPU-time savings obtained with the LW3e and LW3 schemes compared to the RK3 scheme are of the order of 26% and 6% respectively.

The relative error is plotted in Fig 12 as a function of the spatial resolution ( $n = 250, 501, 1002, 1503, 2004, 2505$ ) and of the CPU-time. Results show that all schemes converge to their respective convergence rates. The LW2e<sub>1</sub> scheme converges faster than the other second-order schemes. Results also show that for a given accuracy, the LW2e<sub>1</sub> and LW3e schemes are faster than the other second-order and third-order schemes, respectively. We see that for a give error level, the LW3e scheme provides a computational saving of the order of 26% compared to RK3.

### 5.3 Undular bore

As a third benchmark, we study the propagation over a flat bottom of an undular bore entering at the left of a domain of 100 meters. The spatial step ( $n = 2100$ ) has been chosen to describe the physical oscillations with about 10-20 points. The indexes 1 and 2 correspond to the left and right sides of the undular bore at  $t = 0$ , respectively. The following parameters are those of the paper of Wei et al [21] :

- $h_2 = 0.16$  and  $u_2 = 0$
- $fr = 1.22$  and  $h_1 = 1/2 \times h_2(-1 + \sqrt{1 + 8fr^2})$
- $c_b = u_2 + \sqrt{gh_1/h_2 \times (h_1 + h_2)/2}$  and  $u_1 = c_b - h_2/h_1(c_b - u_2)$

where  $h$  is the water depth,  $u$  is the velocity,  $fr$  is the Froude number and  $c$  is the celerity.

The aim of this benchmark is to highlight the differences between second and third-order schemes, and to study the influence of the Froude number on the numerical results. As in the solitary wave case, nonlinear terms cannot be neglected since their absence results in aberrant oscillations at the front of the bore. Results are compared to a high-resolution computed solution calculated by the

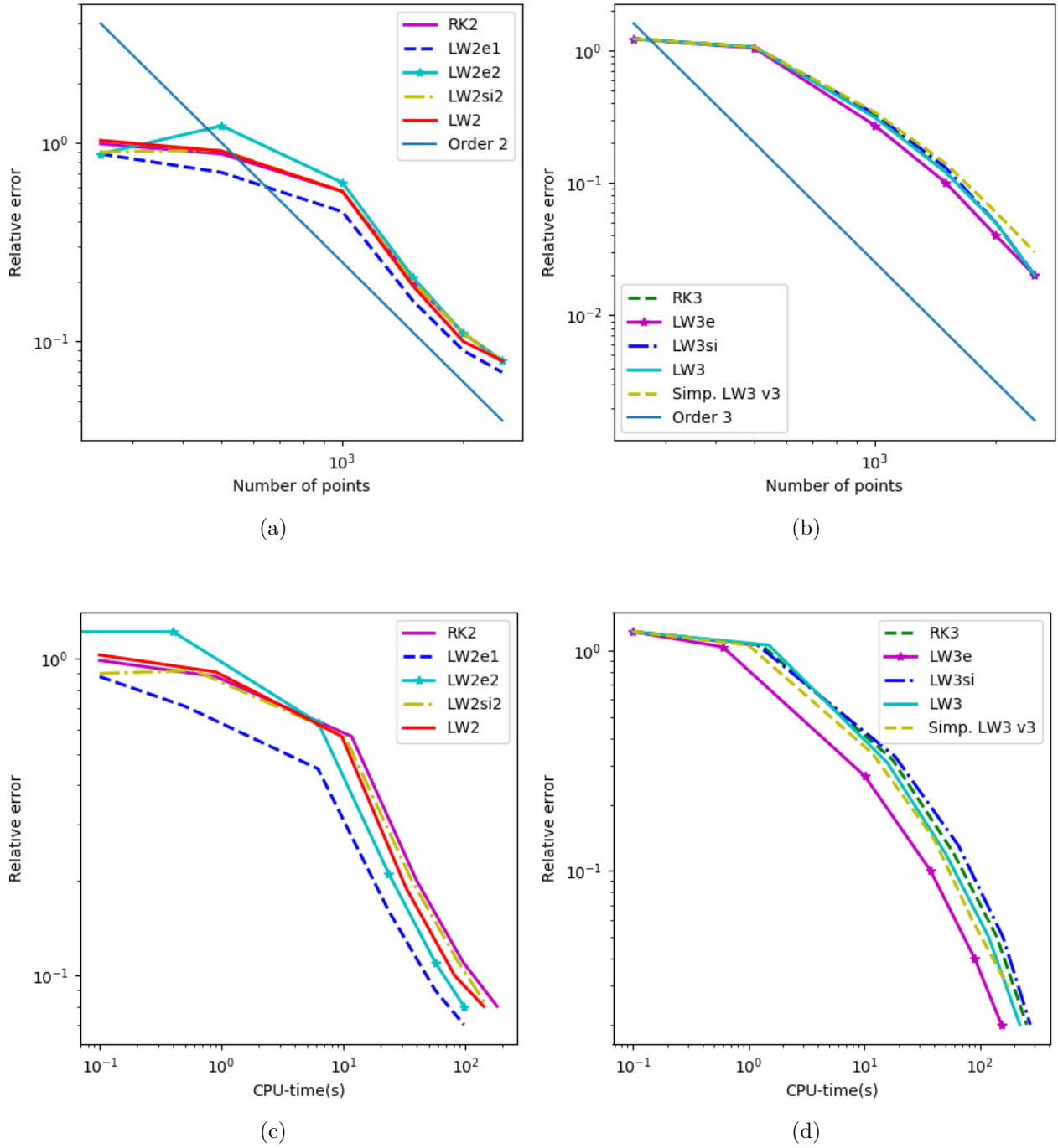


Figure 12: Relative error (in  $L^2$  norm) of the water height calculated in simulations of the propagation of the solitary wave for  $n = 250, 501, 1002, 1503, 2004, 2505$ . The enhanced Boussinesq equations are solved by 12a,12c) second-order schemes, 12b,12d) third-order and simplified LW3 schemes, and compared to a high-resolution computed solution obtained applying RK3 with  $n = 3000$  and  $CFL = 0.49$ . Results are plotted depending on 12a,12b) the number of points of discretization and 12c,12d) the CPU-time. Curves are plotted in logarithmic scale.

RK3 scheme with 2500 points ( $\Delta x = 0.04$  m) and  $CFL = 0.45$ . For our tests, we take a characteristic length of  $l = 4$  m.

Results of second and third-order schemes are presented in Fig 13 at  $t = 0.94, 1.88, 2.82$ . We see that for a given order, the schemes produce similar results. As expected, numerical error increases with the propagation time. The less the order of the scheme, the fastest the numerical error increases. We note that the simplified LW3 scheme gives similar results to the third-order schemes.

The results obtained are similar to the ones calculated with a third order SSP Runge-Kutta or with a fourth order Adams-Bashforth/Adams-Moulton predictor corrector method by Chassagne et al. 2019 [22].

In Fig 14, we present the results obtained with the LW3e, RK3 and simplified LW3 v3 schemes after the simulation of 60 s ( $t = 18.79$ ) of propagation of the wave, a duration long enough for the extreme amplitudes to stabilize (it corresponds to  $t' \sim 400$  for Chassagne [22]). In Fig 14a, we report the heights of the first peak and trough of the wave, and compare them to the experimental data of Favre [24] and Treske [23] for Froude numbers below the transition of wave breaking. All the schemes provide a very good approximation of the data, with only a slight over-prediction of the peak amplitudes from the RK3 schemes for high Froude numbers.

On Fig 14b, we compare the CPU-times in terms of ratio  $CPU\text{-time}/CPU\text{-time}_{RK3}$ . The figure shows that the LW3e and simplified LW3 v3 schemes provide computational time reductions of the order of 37% for the LW3e scheme and 27% for the simplified LW3 v3 one, or even better for some Froude numbers.

As expected, Fig 14a puts in evidence the good accuracy of the numerical results compared to experimental data. We can also see that the differences between the schemes increase with the Froude number. The Fig 14b shows that the Froude number has in general few influence on the computational time, and does not modify the classification of the schemes in term of computational cost.

## 5.4 Dambreak on an ascending slope

As a fourth benchmark, we simulate a dambreak-generated wave propagating over a flat bottom then over a positive slope. The 5 m high wave generated at  $x = 15000$  m firstly propagates over a flat bottom 50 m deep and then propagates over a slope from  $x = 22000$  m until reaching a flat bottom 18 m deep at  $x = 26000$  m. These parameters are close to those of Michel Benoit [25].

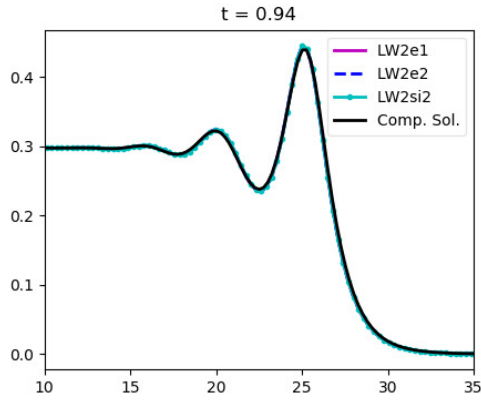
The aim of this benchmark is to test the ability of schemes to propagate strongly nonlinear waves over a variable bottom. Two small spatial steps ( $n = 801, 1601$ ) have been selected to avoid numerical oscillations. Simulations are performed with  $CFL = 0.5$  and  $l = 300$  m, and compared to a high-resolution computed solution calculated with 3101 points ( $\Delta x \simeq 10m$ ) and  $CFL = 0.35$ .

Results for two resolutions are plotted in Fig 15. For a given order and a given resolution, the schemes of same order generate similar results. Surprisingly, second-order schemes tend to be more accurate for the first wave while third-order and simplified LW3 schemes are more accurate for the following wave train.

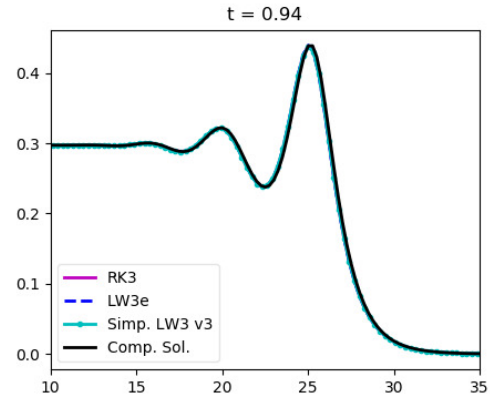
Despite the absence of shock-capturing methods, schemes do not introduce aberrant errors and finally converge to the high-resolution reference solution.

## 5.5 Analysis of the results

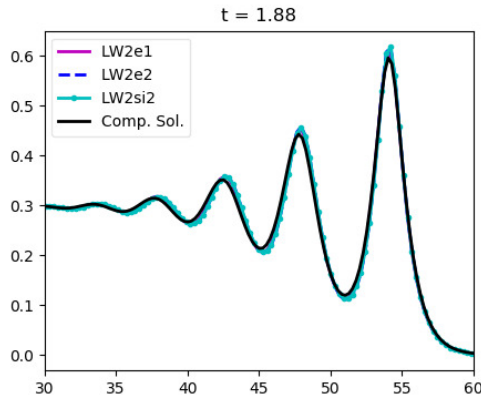
Simulations of these four benchmarks show that:



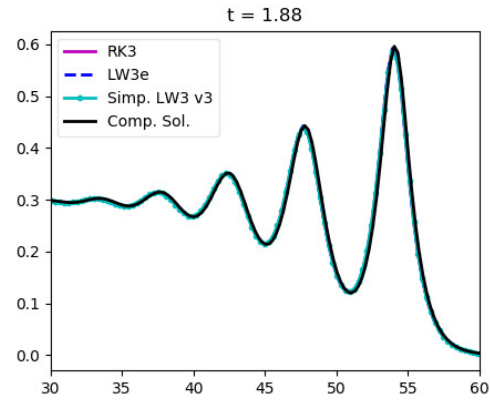
(a)



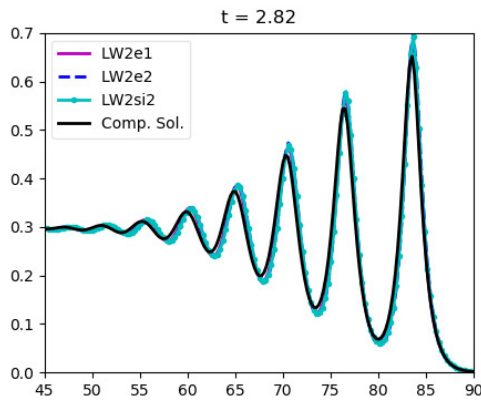
(b)



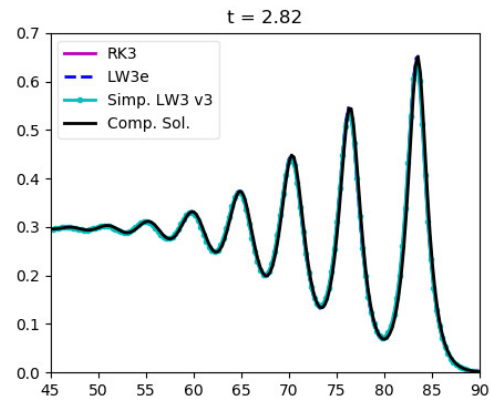
(c)



(d)



(e)



(f)

Figure 13: Propagation of an undular bore at  $t = 0.94$  (13a,13b),  $t = 1.88$  (13c,13d) and  $t = 2.82$  (13e,13f). Nonlinear enhanced Boussinesq equations are solved by 13a,13c,13e) second-order schemes, 13b,13d,13f) third-order and simplified LW3 schemes. Values on x-axis and y-axis are expressed in dimensionless values obtained dividing the dimensional values by  $d_0$ . Comp. Sol. denotes the reference solution obtained applying RK3 with  $n = 2500$  and  $CFL = 0.45$ . We have similar results solving the standard nonlinear Boussinesq equations. RK2, LW2si<sub>2</sub> and LW2 results are similar to the LW2e<sub>2</sub> ones and then not plotted. In the same way, LW3 and LW3si results (identical to the RK3 ones) are not plotted.

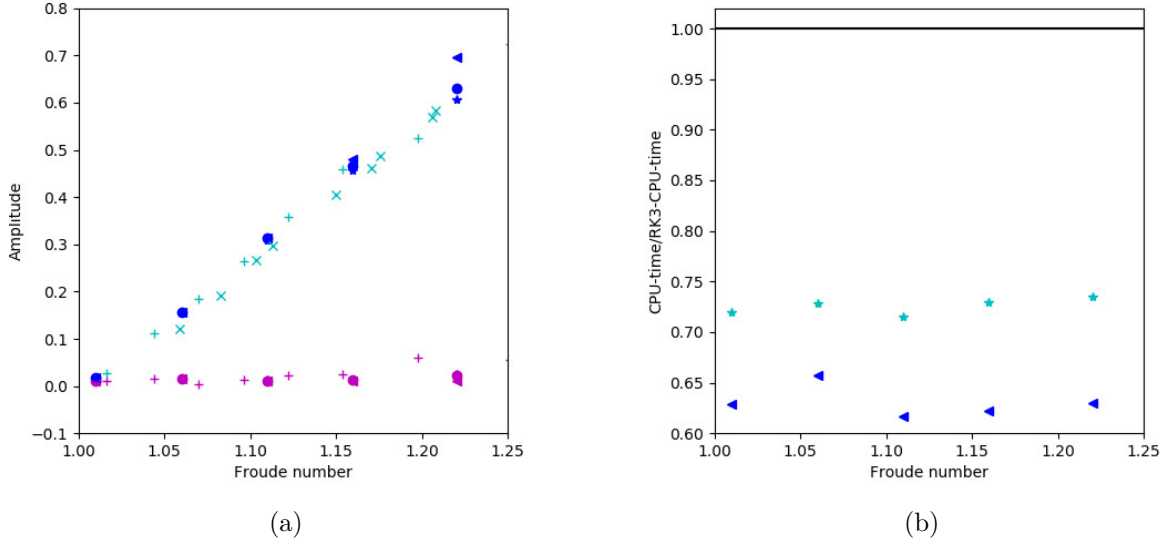


Figure 14: Dependence on the Froude number of 14a) the extremum amplitudes and of the 14b) CPU-time/CPU-time<sub>RK3</sub>. The amplitudes are expressed in dimensionless values obtained dividing the dimensional values by  $d_0$ . The heights of the first peak and trough of the wave are respectively plotted in blue and magenta in Fig 14a. Numerical results are obtained with  $n = 2500$  and  $CFL = 0.5$ . The domain is extended by 10% in the right direction in order to contain the entirety of the wave. Results obtained through the RK3 -  $\circ$ , LW3e -  $\triangleleft$  and simplified LW3 v3 -  $\star$  schemes are plotted. We also plot data of Treske 1994 [23] -  $+$  and data of Favre 1935 [24] -  $\times$  in Fig 14a. In Fig 14b, a black line is plotted as the RK3 reference values.

- As expected, the first order Explicit Euler scheme produces poor results solving the standard or the enhanced Boussinesq equations. Results are not plotted insofar as the associated curves make figures unreadable.
- The LW2si<sub>1</sub> and LW2si<sub>3</sub> schemes are the least accurate second-order schemes, in agreement with the results of the spectral analysis. The implicit LW2si<sub>3</sub> scheme is slower than any other second-order scheme of this article, and even slower than some third-order schemes. Its poor results might be due to the convergence criterion of the scheme. Improving it would only lead to increase the time of computation. The results obtained with these schemes have been omitted since they do not bring any further information, and to simplify the plots.
- As expected from the dispersion relations, benchmarks confirm that the RK2, LW2 and LW2si<sub>2</sub> schemes give similar results. Amongst these schemes, the RK2 scheme is the slowest one, while the LW2 scheme is the most efficient one.
- The inflection points observed in the dispersion curves of the LW2e<sub>1</sub>, LW3e and simplified LW3 schemes seem to have no effect on the results obtained on physical benchmarks.
- The explicit LW2e<sub>1</sub> and LW2e<sub>2</sub> schemes are the fastest second-order schemes. The CPU-time savings of the LW2e<sub>1</sub> and LW2e<sub>2</sub> schemes compared to the RK2 scheme are respectively of the order of 40% and 48% for a given resolution. While the LW2e<sub>1</sub> scheme is the most

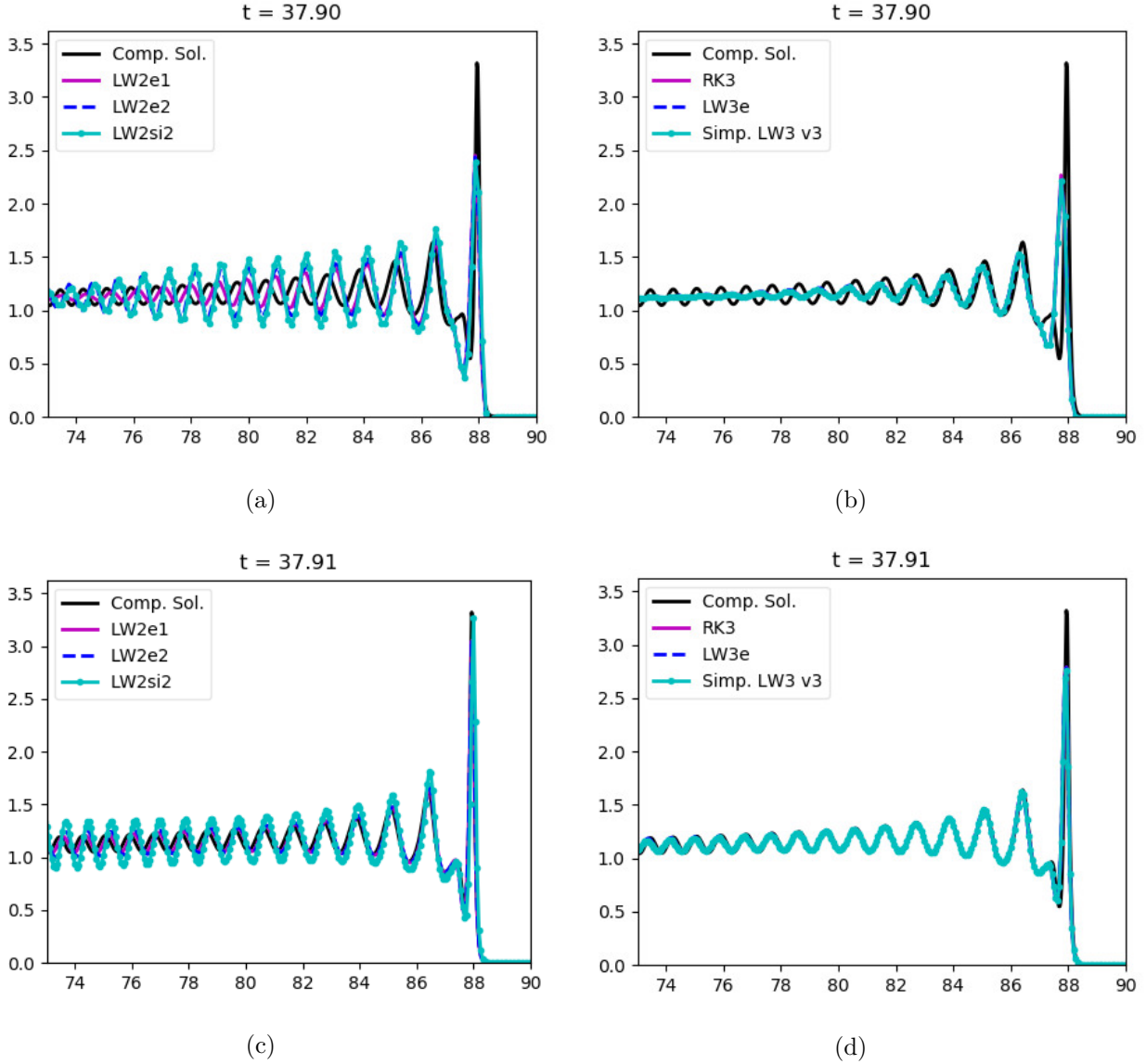


Figure 15: Propagation of a dambreak-generated wave simulated with 15a,15b)  $n = 801$  and 15c,15d)  $n = 1601$  by 15a,15c) LW2e<sub>1</sub>, LW2e<sub>2</sub> and LW2si<sub>2</sub> schemes, 15b,15d) LW3e, LW3 and simplified LW3 schemes solving the enhanced nonlinear Boussinesq equations. Values on x-axis and y-axis are expressed in dimensionless unities. Comp. Sol. denotes the reference solution obtained applying RK3 with  $n = 3101$  and  $CFL = 0.35$ . RK2 and LW2 results are similar to the LW2e<sub>2</sub> ones and then not plotted. RK3 and LW3si results are identical to the LW3 scheme ones and then not plotted.

accurate second-order scheme compared to the Airy and computed solutions, LW2e<sub>2</sub> is the least accurate one of those tested on the benchmarks.

- Despite of its higher dispersion error, the simplified LW3 scheme gives often results comparable to the third order schemes in the four physical benchmarks studied. Among these, the best scheme in terms of both error levels and performance is the LW3e scheme, which outperforms RK3 with CPU reductions up to 37%. The second best scheme is the simplified LW3 v3 scheme with CPU-times reductions compared to the RK3 scheme of the order of 30%. The LW3 and RK3 schemes come after.

## 6 Conclusion

In this paper, we compare the accuracy and computational time of some Lax-Wendroff schemes of second and third-order, an explicit Euler and a simplified third-order Lax-Wendroff schemes, firstly through dispersion relations then applying them to four benchmarks.

This study shows that some terms in Boussinesq equations may be neglected and that inversion of matrices may be replaced by the calculation of temporal derivatives. For large space steps and some benchmarks, this calculation may produce more accurate results compared to the reference solutions.

As regards second-order schemes, temporal derivatives of  $\varphi$  are discretized for the schemes LW2e<sub>1</sub>, LW2e<sub>2</sub>, LW2si<sub>1</sub>, LW2si<sub>2</sub> and LW2si<sub>3</sub>. The LW2e<sub>1</sub> is probably the best compromise between the CPU-time and the accuracy. The LW2e<sub>2</sub> scheme needs further investigation insofar as its CPU-time and accuracy are sometimes better than the ones of the LW2e<sub>1</sub> schemes. Finally, the LW2si<sub>1</sub> and LW2si<sub>3</sub> schemes are ruled out since they are the less accurate and the slowest schemes.

As regards third-order schemes, we can immediately remark that they have generally superior performances than second order ones. Concerning the LW schemes, temporal derivatives of  $\varphi$  are discretized for the schemes LW3e and LW3si. We also define a simplified LW3 scheme in which the third temporal derivative of the velocity is approximated. Results of LW3 and simplified LW3 schemes are similar in the benchmarks, even in the case of propagation with coarse resolution. In terms of computational time, the most efficient schemes are the LW3e scheme and simplified LW3 scheme. The simplified LW3 scheme is slightly slower and less accurate than the LW3e scheme in the benchmarks. It would be interesting to further investigate the results generated by the LW3e and simplified LW3 schemes for very different benchmarks to assess the limitations of the simplified LW3 scheme. The LW3e scheme, the simplified LW3 scheme and the LW3 scheme require respectively one, two and three matrix inversions at each time step. Compared to the RK3 scheme, the computational time of the LW3e and simplified LW3 schemes is reduced by up to 37% and about 30%, respectively. As a consequence, the LW3e scheme could be the best candidate for 2D simulations of real cases.

Future work will involve the use of more complex spatial discretization, such as WENO approximations, as well as the coupling between Boussinesq and Shallow Water equations to handle dry areas and wave breaking [19], [26].

## Annex A

Annex A presents the temporal derivatives of  $\zeta$  and  $w$  involved in the 1D nonlinear Boussinesq dimensionless equations for an arbitrary bottom, the two additional equations required by the nonlinear LW3 scheme and the linear equations used for the spectral analysis.

To evaluate  $\psi = \mu^2\psi_1 = \partial_t\varphi$  and  $\theta = \mu^2\theta_1 = \partial_{tt}\varphi$ , we have added two equations to the system, denoting  $b = hw$  and  $c = \partial_t b = h(\varphi - \partial_x\zeta) - \epsilon w\partial_x b$  :

$$\begin{aligned} \left(1 - \frac{\mu^2 d}{2} \partial_{xx} d\right) \psi - \mu^2 d \partial_x d \partial_x \psi - \mu^2 \alpha d^2 \partial_{xx} \psi &= \mu^2 d \left( \gamma d \partial_{xxxx} b + (1 - 2\beta) \partial_x d \partial_{xxx} b + \frac{1}{2} \partial_{xx} d \partial_{xx} b \right) \\ &- \epsilon [(\varphi - \partial_x \zeta) \partial_x w + w(\partial_x \varphi - \partial_{xx} \zeta)] \\ \left(1 - \frac{\mu^2 d}{2} \partial_{xx} d\right) \theta - \mu^2 d \partial_x d \partial_x \theta - \mu^2 \alpha d^2 \partial_{xx} \theta &= \mu^2 d \left[ \gamma d \partial_{xxxx} c + (1 - 2\beta) \partial_x d \partial_{xxx} c + \frac{1}{2} \partial_{xx} d \partial_{xx} c \right] \\ &- \epsilon [(\psi + \partial_{xx} b) \partial_x w + 2(\varphi - \partial_x \zeta)(\partial_x \varphi - \partial_{xx} \zeta)] \\ &- \epsilon w(\partial_x \psi + \partial_{xxx} b) \end{aligned}$$

The linear limit of the system used for the spectral analysis writes as:

$$\begin{cases} \partial_t \zeta + \partial_x w &= 0 \\ \partial_t w + \partial_x \zeta &= \mu^2 \varphi_1 \\ \varphi_1 - \mu^2 \alpha \partial_{xx} \varphi_1 &= -\gamma \partial_{xxx} \zeta \end{cases}$$

where  $\varphi = \mu^2 \varphi_1$ .

The LW scheme is obtained by replacing the temporal derivatives by terms non dependent on time in the two first equations of the system. The second order time accurate scheme requires an additional equation to be solved:

$$\psi_1 - \mu^2 \alpha \partial_{xx} \psi_1 = \gamma \partial_{xxxx} w \quad (14)$$

In the same way, the third order scheme requires the calculation of  $\psi_1$  ( Eq 14 ) and  $\theta_1$  defined by  $\theta = \partial_{tt}\varphi$  :

$$\theta_1 - \mu^2 \alpha \partial_{xx} \theta_1 = -\gamma \partial_{xxxx} \zeta + \mu^2 \gamma \partial_{xxxx} \varphi_1$$

## Annex B

In this Annex, we present the dimensionless dispersion relations used in this paper. The first two relations are obtained from the Airy equations and the enhanced Boussinesq equations, respectively.

The dimensionless dispersion relation of the Airy equations writes as :

$$\omega_{Airy}^2 = \frac{2\pi}{\mu} \tanh(2\pi\mu)$$

where  $\omega$  is the frequency of the wave and  $\mu$  is the frequential dispersion parameter.

The dimensionless dispersion relation of the enhanced Boussinesq equations writes as :

$$\omega_{Bsq}^2 = (2\pi)^2 \frac{1 + \beta(2\pi\mu)^2}{1 + \alpha(2\pi\mu)^2}$$

where  $\alpha$  and  $\beta$  are constants associated to the dispersion and  $\gamma = \alpha - \beta$ .

The following relations are obtained for six numerical schemes by expressing each variable X (u and  $\eta$ ) in the form  $X_0 e^{i(2\pi x - \nu t)}$ , where  $X_0$  is a constant,  $\nu = \omega + i\xi$ ,  $\omega$  is associated to the dispersion and  $\xi$  is associated to the diffusion.

### Explicit Euler

$$\begin{aligned}\omega^2 &= Nc^2 \arctan^2 \left( \frac{\omega_{Bsq}}{Nc} \right) \\ \xi &= \frac{Nc}{2} \ln \left( 1 + \left( \frac{\omega_{Bsq}}{Nc} \right)^2 \right)\end{aligned}$$

where  $Nc = 1/\Delta t$ .

### LW2 and RK2

$$\begin{aligned}\omega^2 &= Nc^2 \arctan^2 \left( -\frac{\omega_{Bsq}}{Nc} \frac{1}{1 - \frac{1}{2} \left( \frac{\omega_{Bsq}}{Nc} \right)^2} \right) \\ \xi &= \frac{Nc}{2} \ln \left[ \left( 1 - \frac{1}{2} \left( \frac{\omega_{Bsq}}{Nc} \right)^2 \right)^2 + \left( \frac{\omega_{Bsq}}{Nc} \right)^2 \right]\end{aligned}$$

### Approximate LW2

$$\begin{cases} 0 &= x^2(2y^2 - 1) + Exy + 1 + \frac{\omega_{Bsq}^2}{2Nc^2} + \frac{\pi^2}{Nc^2} \left[ -2 + \frac{\omega_{Bsq}^2}{Nc^2} - 2HP(x, y) \right] \\ y &= -\frac{E}{2x} - HJ \frac{\pi^2}{(Nc x)^2} \\ \omega &= Nc \arccos(y) \\ \xi &= Nc \ln(x) \end{cases}$$

where D, E, H and J are constants expressed as :  $\psi^n = D\varphi^n$ ,  $E = -2 + \frac{1}{2Nc^2} [(2\pi)^2 + \omega_{Bsq}^2]$ ,  $H = \frac{\gamma(2\pi\mu)^2}{1 + \alpha(2\pi\mu)^2}$ ,  $\text{Im}(D) = Nc\sqrt{1 - y^2}J$ , and a polynomial  $P(x,y) = \frac{1}{Nc} \text{Re}(D)$ .

### LW3 and RK3

$$\begin{aligned}\omega^2 &= Nc^2 \arctan^2 \left( -\frac{\omega_{Bsq}}{Nc} \frac{1 - \frac{1}{6} \left( \frac{\omega_{Bsq}}{Nc} \right)^2}{1 - \frac{1}{2} \left( \frac{\omega_{Bsq}}{Nc} \right)^2} \right) \\ \xi &= \frac{Nc}{2} \ln \left[ \left( 1 - \frac{1}{2} \left( \frac{\omega_{Bsq}}{Nc} \right)^2 \right)^2 + \left( \frac{\omega_{Bsq}}{Nc} \right)^2 \left( 1 - \frac{1}{6} \left( \frac{\omega_{Bsq}}{Nc} \right)^2 \right)^2 \right]\end{aligned}$$

### Approximate LW3

$$\left\{ \begin{array}{l} 0 = (\text{Nc } x)^2(2y^2 - 1) + \text{Nc } xy \left[ I - \frac{2J\pi^2}{3\text{Nc}^2} \text{Re}(D) + H \right] \\ \quad - \frac{2J\pi^2 x \sqrt{1-y^2}}{3\text{Nc}} \text{Im}(D) + H \left[ I - \frac{2J\pi^2}{3\text{Nc}^2} \text{Re}(D) \right] + M \left[ M\omega_{Bsq}^2 - \frac{2J\pi^2}{\text{Nc}} \left( \frac{1}{3\text{Nc}} \text{Re}(E) + \text{Re}(D) \right) \right] \\ 0 = 2x^2 \text{Nc}^2 y \sqrt{1-y^2} + \text{Nc } x \sqrt{1-y^2} \left[ I - \frac{2J\pi^2}{3\text{Nc}^2} \text{Re}(D) + H \right] \\ \quad + \frac{2J\pi^2 xy}{3\text{Nc}} \text{Im}(D) + \frac{2JH\pi^2}{3\text{Nc}^2} \text{Im}(D) + \frac{2MJ\pi^2}{\text{Nc}} \left( \frac{1}{3\text{Nc}} \text{Im}(E) + \text{Im}(D) \right) \\ \omega = \text{Nc } \arccos(y) \\ \xi = \text{Nc } \ln(x) \end{array} \right.$$

where  $D$ ,  $E$ ,  $H$ ,  $I$ ,  $J$  and  $M$  are constants defined by  $\psi^n = D\varphi^n$ ,  $\theta^n = E\varphi^n$ ,  $H = -\text{Nc} + \frac{2\pi^2}{\text{Nc}}$ ,  $I = -\text{Nc} + \frac{1}{2\text{Nc}}\omega_{Bsq}^2$ ,  $J = \frac{\gamma(2\pi\mu)^2}{1 + \alpha(2\pi\mu)^2}$  and  $M = 1 - \frac{2\pi^2}{3\text{Nc}^2}$ .

### Simplified LW3

$$\begin{aligned} \omega &= \text{Nc } \arccos \left[ \left( 1 - \frac{1}{2} \frac{\omega_{Bsq}}{\text{Nc}} \right) e^{-\xi/\text{Nc}} \right] \\ \xi &= \frac{\text{Nc}}{2} \ln \left[ \left( 1 - \frac{1}{2} \left( \frac{\omega_{Bsq}}{\text{Nc}} \right)^2 \right)^2 + \frac{1}{\text{Nc}^2} \left( 1 - \frac{1}{6} \frac{\omega_{Bsq}^2}{\text{Nc}^2} \right) \left( \omega_{Bsq}^2 - \frac{1}{6} \left( \frac{2\pi}{\text{Nc}} \right)^2 \omega_{Bsq}^2 + \frac{\gamma}{6\text{Nc}} \frac{(2\pi\mu\omega_{Bsq})^2}{1 + \alpha(2\pi\mu)^2} \right) \right] \end{aligned}$$

### Conflict of interest

On behalf of all authors, the corresponding author states that there is no conflict of interest.

### References

- [1] Glimsdal S., Pedersen G., Harbitz C., and Lvholt F. Dispersion of tsunamis: Does it really matter? *Natural Hazards and Earth System Sciences*, 13:1507–1526, 06 2013.
- [2] Heinrich P., Jamelot A., Cauquis A., and Gailler A. Taitoko, an advanced code for tsunami propagation, developed at the French Tsunami Warning Centers. *European Journal of Mechanics - B/Fluids*, 88, 03 2021.
- [3] Kirby J.T., Shi F., Tehranirad B., Harris J.C., and Grilli S.T. Dispersive tsunami waves in the ocean: Model equations and sensitivity to dispersion and Coriolis effects. *Ocean Modelling*, 62:39–55, 2013.
- [4] Fengyan Shi, James T. Kirby, Jeffrey C. Harris, Joseph D. Geiman, and Stephan T. Grilli. A high-order adaptive time-stepping TVD solver for Boussinesq modeling of breaking waves and coastal inundation. *Ocean Modelling*, 43-44:36–51, 2012.

- [5] T Baba, S Allgeyer, P.R Cummins, H Tsushima, K Imai, and T Kato. Accurate numerical simulation of the far-field tsunami caused by the 2011 Tohoku earthquake, including the effects of Boussinesq dispersion, seawater density stratification, elastic loading, and gravitational potential change. *Ocean Model*, 111:46–54, 2017.
- [6] Yoshiki Yamazaki, Kwok Fai Cheung, and Zygmunt Kowalik. Depthintegrated, nonhydrostatic model with grid nesting for tsunami generation, propagation, and runup. *International Journal for Numerical Methods in Fluids*, 67:2081 – 2107, 12 2011.
- [7] Jorge Macas, Manuel Castro, Sergio Ortega, Cipriano Escalante Snchez, and Jos Gonzlez Vida. Performance benchmarking of tsunami-HySEA model for NTHMP’s inundation mapping activities. *Pure and Applied Geophysics*, 174:1–37, 08 2017.
- [8] D. H. Peregrine. Long waves on a beach. *Journal of Fluid Mechanics*, 27(4):815827, 1967.
- [9] Per A. Madsen and Ole R. Srensen. A new form of the Boussinesq equations with improved linear dispersion characteristics. part 2. a slowly-varying bathymetry. *Coastal Engineering*, 18(3):183–204, 1992.
- [10] O.Nwogu. Alternative form of Boussinesq equations for nearshore wave propagation. *Journal of Waterway Port Coastal and Ocean Engineering-ASCE*, pages 618–638, 1993.
- [11] Wei Ge and Kirby James T. Time-dependent numerical code for extended boussinesq equations. *Journal of Waterway, Port, Coastal, and Ocean Engineering*, 121, September 1995.
- [12] Young-Kwang Choi, F. Shi, M. Malej, and J. M. Smith. Performance of various shock-capturing-type reconstruction schemes in the Boussinesq wave model, funwave-tvd. *Ocean Modelling*, 131:86–100, 2018.
- [13] K. Erduran, S. Ilic, and V. Kutija. Hybrid finitevolume finitedifference scheme for the solution of Boussinesq equations. *International Journal for Numerical Methods in Fluids*, 49:1213 – 1232, 12 2005.
- [14] Volker Roeber, Kwok Fai Cheung, and Marcelo Kobayashi. Shock-capturing Boussinesq-type model for nearshore wave processes. *Coastal Engineering*, 57:407423, 04 2010.
- [15] M. Kazolea and A.I. Delis. A well-balanced shock-capturing hybrid finite volume-finite difference numerical scheme for extended 1d Boussinesq models. *Applied Numerical Mathematics*, 67:167–186, 2013.
- [16] Sasan Tavakkol, Sangyoung Son, and Patrick Lynett. Adaptive third order Adams-Bashforth time stepping scheme for 2d extended Boussinesq equations. 09 2021.
- [17] Pedersen G. and Lovholt F. Documentation of a global Boussinesq solver. Preprint series in applied mathematics 1, Dept. of Mathematics, University of Oslo, Norway. 2008.
- [18] Madsen P.A. and Schäffer H. A review of Boussinesq-type equations for surface gravity waves. 1999.
- [19] Andrea Filippini, Maria Kazolea, and Mario Ricchiuto. A flexible genuinely nonlinear approach for wave propagation, breaking and runup. *Journal of Computational Physics*, 310, 06 2015.

- [20] Kazolea M. and Ricchiuto M. Wave breaking for Boussinesq-type models using a turbulence kinetic energy model. *hal-01284629*, 2016.
- [21] Ge Wei, James T. Kirby, Stephan T. Grilli, and Ravishankar Subramanya. A fully nonlinear boussinesq model for surface waves. part 1. highly nonlinear unsteady waves. *Journal of Fluid Mechanics*, 294:7192, 1995.
- [22] Chassagne R., Filippini A., Ricchiuto M., and Bonneton P. Dispersive and dispersive-like bores in channels with sloping banks. *Journal of Fluid Mechanics*, 870:595–616, 07 2019.
- [23] Andreas Treske. Undular bores (favre-waves) in open channels - experimental studies. *Journal of Hydraulic Research*, 32:355–370, 1994.
- [24] Henry Favre. *Étude théorique et expérimentale des ondes de translation dans les canaux découverts*, volume Dunod. 1935.
- [25] Benoit Michel, Dias F., Herterich J, and Scolan Yves-Marie. Un cas-test discriminant pour la simulation de la propagation et du run-up de trains de vagues de type tsunami. Actes des 16èmes journées de l’hydrodynamique, Marseille. *hal-02121203*, Nov 2018.
- [26] Paola Bacigaluppi, Mario Ricchiuto, and Philippe Bonneton. Implementation and evaluation of breaking detection criteria for a hybrid boussinesq model. *Water Waves*, 2(2):207–241, 2020.

## Availability of data and material

Data sharing not applicable to this article as no datasets were generated or analysed during the current study.